

Synthesis of ZnO Nanoparticles using environmentally friendly Zinc-Air System

Author: T D Malevu

Supervisor: R O Ocaya

A dissertation submitted to the Department of Physics, Faculty of Natural and Agricultural Sciences, in fulfilment for degree of Masters in Nanoscience

Department of Physics, University of the Free State, January 2015.

DECLARATION

I hereby declare that the work contained in this dissertation is entirely my own and where necessary credit is given to materials and sources that have been referred to.

Dedicated to my family

Acknowledgements

Pursuing this study has been an exciting and enjoyable journey largely due to the good support I have received. Many credits go to various individuals for their efforts, even though they are not mentioned directly. I am grateful for the support and knowledge that I have gained over the last two years.

First of all I would like to pay my appreciation to my supervisor R.O Ocaya, for his patient guidance, support and constant encouragement. I have been astonished to have such a mentor who gave me a room to explore things on my own way and at the same time the guidance to recover when my steps faltered.

I would also like to thank my parents K.M Malevu, S.N Hlatshwayo and J.J Malevu, my daughter Lubambo Malevu and her mom Mollo Lerato for their valuable support, love and understanding. I thank the staff and students of the Departments of Physics and Chemistry, particularly Wako A.H, Mr Lotha T.L., Molefe F.V., Tebele A.S. and Clarke C. (Chemistry) for all assistance rendered.

Many thanks go to the South African Institution of Physics (SAIP) for bestowing upon me the honor of *Best M.Sc Poster presentation* at the SAIP 2014 meeting at the University of Johannesburg.

It would not have been possible to carry out this research without the financial support of the National Nanoscience Postgraduate Teaching and Training Platform (NNPTTP) and University of the Free State.

Above all to the Lord, God. May your Name always be praised.

Table of Contents

Declaration	ii
Acknowledgements	iv
Table of Contents	v
List of Figures	viii
List of Tables	ix
Abstract	x
1 Introduction	1
1.1 Background of the research	1
1.1.1 What are nanomaterials?	3
1.1.2 Metal oxide based nanoparticles	6
1.2 The research question	8
1.2.1 Aims and objectives	9
1.3 Outline of the dissertation	9
2 A Review of the Literature	11
2.1 Background of zinc oxide nanoparticles	11
2.1.1 Crystal and surface structure of ZnO	12
2.1.2 Electronic properties of ZnO	15
2.1.3 Optical properties of ZnO	16
2.1.4 Chemical properties of ZnO	18
2.2 Methods of synthesizing ZnO nanoparticles	19
2.2.1 Vapor Transport Synthesis (VTS)	21
2.2.2 Sol-Gel method (SG)	22
2.2.3 Pulsed laser deposition (PLD)	22
2.2.4 Chemical bath deposition (CBD)	22
2.2.5 The zinc-air system (ZACs)	23
2.2.6 Role of separator and electrolyte	24

3	Construction and characterization of products	25
3.1	Fabrication of the ZACs	25
3.1.1	The electrolyte solution	27
3.2	Proposed method for ZAC electrical characterization	27
3.2.1	Open-circuit voltage characterization	29
3.2.2	Closed-circuit voltage characterization of ZAC	30
3.3	Surface, morphology and optical properties	32
3.3.1	An overview of standard characterization methods	32
3.3.2	X-ray diffraction (XRD)	33
3.3.3	Scanning electron microscopy (SEM)	37
3.3.4	Energy Dispersive X-ray Spectrometry (EDS)	38
3.3.5	UV-Vis spectrometer	40
4	Effects of electrolyte concentration	42
4.1	Introduction	42
4.2	Characterization	42
4.2.1	Structural analysis using XRD	43
4.2.2	Surface morphology by SEM	46
5	Effects of annealing temperature	50
5.1	Introduction	50
5.2	Experimental	52
5.2.1	Synthesis and annealing	52
5.2.2	Characterization	52
5.3	Results and discussion	52
5.3.1	Structural characterization	52
5.3.2	Surface and chemical composition characterization	56
5.3.3	Band gap estimation using UV-VIS spectrometer	56
6	Conclusions	61
6.0.4	Publications	63
	Appendix	64
	Index	79
	References	64

List of Figures

1.1	Some potential applications of nanomaterials to electronics: (a) molecular electronics (b) usage in nano-organic electronics. . .	2
1.2	Graphical representation of a material scale [14].	3
1.3	Categories of the nanoparticles present in the environment [18].	4
1.4	Applications of nanoparticles [21].	5
1.5	The number of ZnO-related research papers published between 2004 to 2014 [42]	8
2.1	Wurtzite structure model of ZnO. The tetrahedral coordination of Zn-O is shown. Wang [44]	13
2.2	The zincblende (left) and rock salt (right) phases of ZnO. . . .	14
2.3	Distribution of polar charges over the surface with the sequencing arrangement of AaBbAa in c-axis	15
2.4	Top-down and bottom-up approaches in nanotechnology [67] .	21
3.1	Zinc plate after washing	26
3.2	Schematic diagram of the apparatus used to synthesize ZnO nanostructures by ZACs	28
3.3	Circuit illustrations of thevenin's (a) and Norton's (b) theorems	29
3.4	Twelve-hour measurements for open circuit voltage of ZACs .	30
3.5	Behavior of the cell at different electrolyte concentraions . . .	31
3.6	Resistance measurement	32
3.7	Power behavior of a cell	33
3.8	Optimum concentrations for ZAC system	34
3.9	Bragg's law derivation.	35
3.10	Continuous and characteristic spectra [81]	36

3.11	Operation of the SEM instrument. [81]	38
3.12	Typical EDS spectra. [86]	39
3.13	Operation of the UV-Vis instrument [87].	41
4.1	XRD patterns of the Zn anode after the synthesis at different NaOH concentrations of (a) 0.4M (b) 0.5M (c) 0.6M (d) 1M and 2M:	44
4.2	SEM micrographs at different electrolyte concentrations (a) 0.4M NaOH (b) 0.5M NaOH (c) 0.6M NaOH (d) 1M NaOH (e) 2M NaOH	48
4.3	Estimation of nano needles length	49
5.1	XRD pattern of ZnO nanostructures synthesized at different temperatures	53
5.2	Effect of temperature on particle intensity	54
5.3	Effect of temperature on particle size	55
5.4	SEM images before/after annealing (a) before (b) 400 °C (c) 450 °C (d) 500 °C and (e) 600 °C	58
5.5	Chemical compositions of ZnO nanoneedles	59
5.6	UV-Vis absorbance spectra of annealed ZnO nanoneedles.	59
5.7	Plot of $(F(R)*hv)^{0.5}$ vs. photon energy (hv) of ZnO nanoneedles	60

List of Tables

2.1	Some physical properties of ZnO at ambient temperature and pressure.	12
4.1	Effect of electrolyte concentration on the ZnO lattice parameters.	46
5.1	Effect of annealing temperature on lattice parameters	56

Abstract

Zinc-air batteries have high specific energy, environmental compatibility and use low-cost materials. They have long been considered to be attractive as potential power sources for electronic applications. In the operation of these batteries, zinc oxide (ZnO) is formed as a byproduct. The present study investigates the form of the ZnO produced and suggests the potential of the method to synthesize ZnO nanostructures. Current methods of synthesizing ZnO nanostructures are expensive and complex, while requiring good vacuum and high temperatures. They are corrosive and evolve high toxic gasses. We present an on-going research that investigates the feasibility of producing ZnO nanostructures using an electrochemical, zinc-air cell system that is also a voltage generator. The electrolyte used in the study is readily available lye or sodium hydroxide (NaOH). The measured parameters are electrolyte concentration, zinc plate size, open-circuit cell voltage and discharge time into a calibrated load. The experimental has two aspects. The first aspect is the measurement of the output cell voltage versus electrolyte concentration and cell voltage output at constant ohmic load. The second aspect is the surface characterization of the zinc electrode substrate using SEM, EDS, UV-Vis and XRD techniques to investigate the formation of ZnO as a function of electrolyte concentration. Conclusions are then drawn by correlating the electrical performance of the cell in the first part versus the surface products formed in the second part. The potential application of the study is therefore twofold; firstly, we suggest the study as an alternative to large scale manufacture of ZnO and secondly, we suggest a way to optimize the power output of the cell as a function of the surface products formed. A layer of well-aligned zinc oxide (ZnO) nano-needles was synthesized on a zinc plate at room temperature using

an environmentally friendly zinc-air cell system (ZACs). The zinc plate was the anode, and the air cathode was composed of steel wire. A porous void-paper separated the electrodes and in the presence of a low concentration NaOH electrolyte also formed the medium of transferring electrons from the anode to the cathode. In this study, the open-circuit voltage, V_{oc} , were monitored as a function of the electrolyte concentration. The electrolyte concentrations were varied from 0.4M to 2M. The measured values of V_{oc} were approximately 1.2V for all the five different concentrations used. The effect of concentration on orientation and lengthwise growth of the synthesized ZnO nano-needles were determined through scanning-electron microscopy (SEM) and X-ray diffraction (XRD). It was found that the growth and orientation of the resulting ZnO nano-needles is highly dependent on the electrolyte concentration. The SEM images show good length properties of nano-needles with average sizes between 780 nm and 2200 nm. In addition, using XRD, UV-VIS spectrometry (UV-vis) and Field Emission Scanning electron microscopy (FE-SEM) techniques the effects of varying the annealing temperature from 400°C to 600°C on the structure, morphology and optical properties of the synthesized ZnO nano-needles were also investigated. XRD measurements indicated that the synthesized ZnO nano-needles exhibit the hexagonal wurtzite structure with no impurities. In general, with the annealing the particle size increased and the nano-needles became more orientated with average height between 538.1 nm and 1195 nm. Ultraviolet-Visible (UV-Vis) spectroscopy showed a slight decrease in absorbance and the absorption edge shifted slightly to lower energy. The apparent increase in the band gap energy was from 3.29 to 3.30 eV over the temperature range, although it cannot be reliably attributed to adverse effects such as high-temperature defect formation since it is within the measurement uncertainty 2%. The nano-needles exhibit strong absorption peaks, in the wavelength range of \approx 360nm to 380nm. The peaks appear to decrease with annealing temperature with increased crystallization strength. The absence of impurities after annealing was confirmed using Energy Dispersive Spectroscopy (EDS). Overall the ZAC method appears to be a feasible alternative method to produce ZnO nanostructures.

Chapter 1

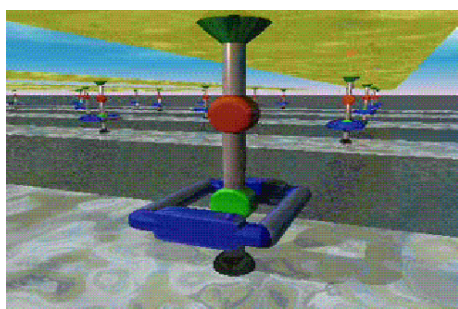
Introduction

1.1 Background of the research

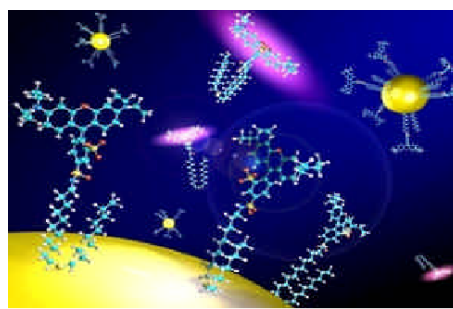
In 1959 Richard Feynman gave a talk implying the emergence of nanotechnology. According to him “there is plenty of room at the bottom”. With his talk, he laid a concrete foundation for the current research in the development of new technology of the very small. However, the term nanotechnology was only coined in 1974 by Norio Taniguchi. He described nanotechnology mainly as consisting of the processing of separation, consolidation, and deformation of materials by one atom or one molecule.

In this chapter an overview of nanotechnology, nanomaterials and nanoparticles is given alongside attempts to answer some commonly asked questions such as what nanotechnology is and what nanomaterials and nanoparticles are. The kinds of properties that these materials possess for them to be considered good and promising candidates for the development of electronic devices such as sensors, light emitting diodes (LEDs) and so on are also discussed. According to Nowack and Bucheli [1], nano-sized materials have been employed by mankind for thousands of years and nano particles themselves have been in existence for millions of years up to the present, for instance as halloysite clay nanotubes. Nanoparticles have been unwittingly applied by mankind for centuries. The earliest known use of nanomaterials was probably in a Roman cup called the

Lycurgus cup which is coated with gold nanoparticles. When illuminated with light the cup produces different colors depending on the position of the light source [2]. Carbon black is another prominent example of a common nanoparticle material that was known since ancient times. It is widely used in materials such as printing ink, plastics and building products [3]. There are other well-known and widely applied nanoparticle-based materials. Examples of such materials are found in personal care products, sporting goods, electronics and the automotive industries. Nanoparticle-based materials are expected to be at the heart of the future market, particularly in the chemical and health care sectors [1, 4–10]. The unique properties of these nanomaterials due to their extremely small size, morphology and their ability to be tuned in size and shape by the synthesis method, have attracted tremendous research attention around them [11, 12]. At present, nanoscale materials are being employed in various sectors of science, biomedicine, pharmaceuticals, cosmetics, energy and environmental studies and electronics as shown in Figure 1.1 [1, 5–7]. The fabrication of molecular devices in electronics is one of the most studied, current focus areas of application according to Deng [13]. However, one major concern remains the elapsed time between the first synthesized nanomolecules to the appearance of the first electronic devices with practical functionality.



(a)



(b)

Figure 1.1: Some potential applications of nanomaterials to electronics: (a) molecular electronics (b) usage in nano-organic electronics.

1.1.1 What are nanomaterials?

Nanomaterials are chemical compounds with particle sizes between 1 and 100 nanometers. To appreciate the nano-scale, one millionth of a millimeter is approximately 100,000 times smaller than the diameter of a human hair as shown in Figure 1.2 [14], whereas a red blood cell is approximately 7000 nm wide [15]. Particles that can only be viewed under very high electron magnification techniques and have particle sizes that range between 1 and 100 nm are classified as nanoparticles [16, 17]. Nanoparticles are in general considered to be materials that have dimensions in the nanoscale in at least two dimensions i.e. particles as well as fibrous materials and tubes but not materials which are nano-sized in only one dimension, such as coatings, films and multilayers [3].



Figure 1.2: Graphical representation of a material scale [14].

Owing to the unique optical, magnetic and electrical properties that these nanomaterials exhibit at the nanoscale, nanomaterials have great potential in fields such as electronics, medicine and others. However, the properties vary from material to material and also on the manufacturing technique. Nanomaterials may be classified broadly into two categories i.e. naturally occurring or engineered (synthetic). According to Bhatt & Tripathi [18] these categories are further divided into several classes such as carbonaceous nanomaterials, metal oxides, semi-conductor materials, zero-valent metals and nanopolymers as shown in Figure 1.3. In this research we shall concentrate

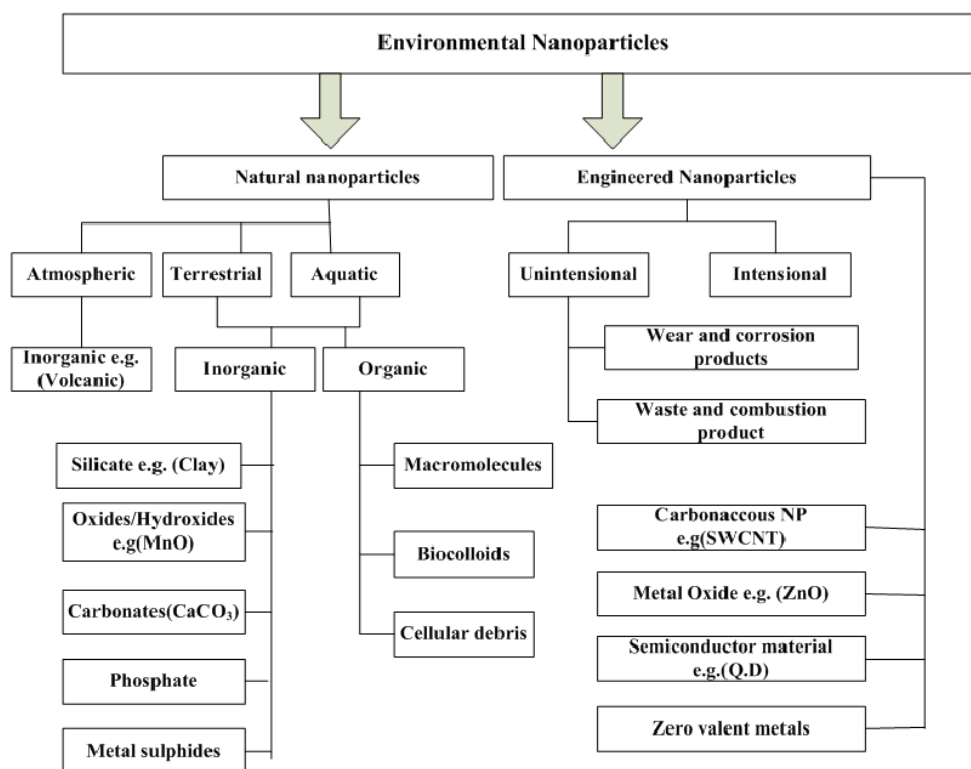


Figure 1.3: Categories of the nanoparticles present in the environment [18].

on engineered nanomaterials in the range of 1 to 100 nm in order to obtain the desired structure that will serve the particular application. Engineered nanomaterials with small particle sizes have much greater surface area to volume ratio than their bulk materials. This leads to greater chemical reactivity and also affects their mechanical strength [19]. Also, at the nanoscale, quantum

size effects occur as a result of *electron confinement*. These effects can be used in highlighting the material properties and other characteristics [14, 20].

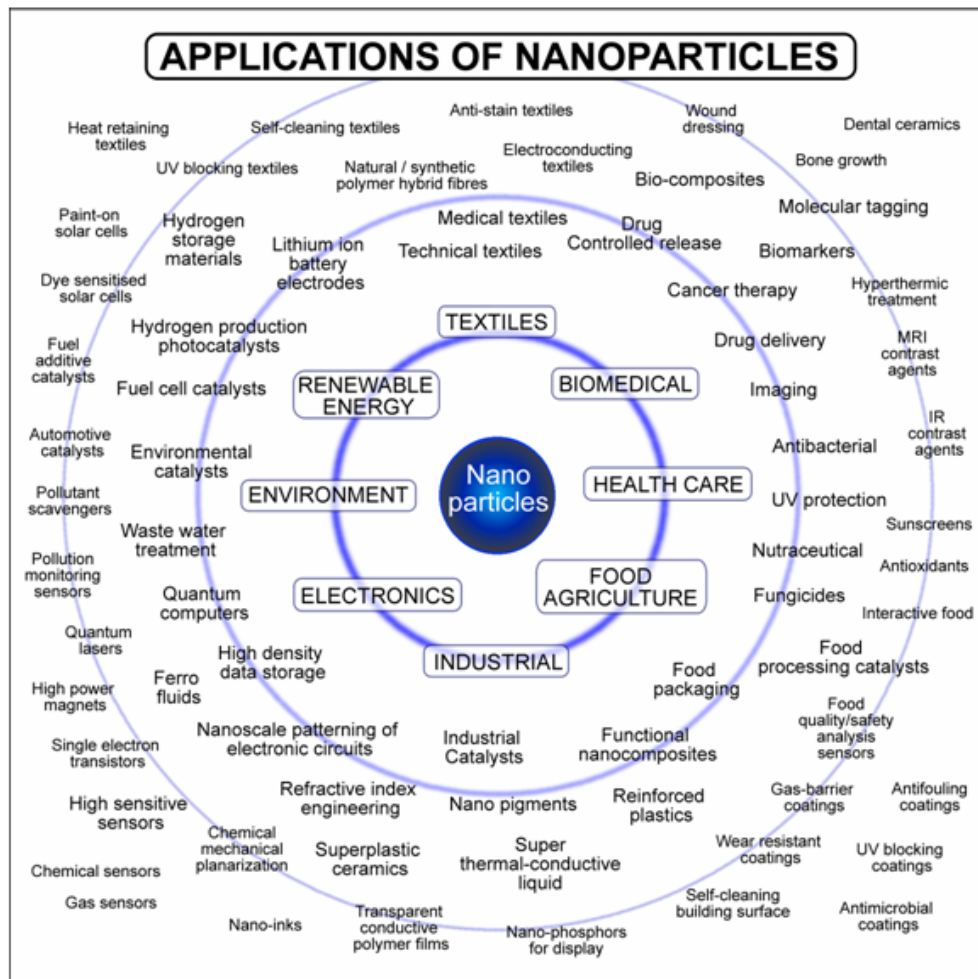


Figure 1.4: Applications of nanoparticles [21].

To summarize, based on their unique properties they can be applied in different fields as shown in Figure 1.4. The development of nanomaterials and the research conducted in the existing sphere of nanotechnology is regarded as the driving force for existing nanotechnology based sectors. In the next section a background of nanoparticles that are based on metal oxides is presented.

1.1.2 Metal oxide based nanoparticles

The most commonly studied class of nanoparticles is metal oxides nanoparticles largely because of the abundance of oxide forming metals in nature. Due to the unique properties of metal oxide nanomaterials, such as optimized optical, gas sensing abilities and electrical properties, they have drawn much research interest during the past two decades [22]. It is found that devices that are made of metal oxides possess new optical and electronic properties when fabricated at the nanoscale in contrast to the microscale due to changes in their chemical, physical and electrical properties. It is these changes that make these materials potential candidates for technological applications [23].

Metal oxide nanomaterials play a crucial role in the fabrication of microelectronic circuits, sensors, piezoelectric devices, fuel cells, coatings for the passivation of surfaces against corrosion, and in chemical catalysts [24,25]. Specifically, they are used in energy production e.g. CuO rectifiers, data storage e.g. giant magnetoresistive recording (GMR), and medicine e.g. drug delivery and cancer therapy [3,26]. With the decrease in particle sizes down to the nano scale, there is a dramatic increase in the surface to volume ratio. There is an associated increase in the density of the surface sites for photon absorption and chemical reactions. The optical properties of metal oxide nanomaterials are caused by the increase in the band gap of the material through a process called *size quantization* [27]. When particle size decreases to the nanoscale, there is a fine tuning of the electrical characteristics of the metal oxide [22,28,29].

Due to the wide applications of these nanoparticles, different methods are employed to synthesize them. Metal nanoparticles can be synthesized by various processes including laser ablation (LA) [30], chemical vapor deposition (CVD) [31], chemical vapor condensation (CVC) [32], thermal decomposition (TD) [33], combustion (C) [34], and wet chemical reduction (WCR) of the

corresponding metal salts. These methods are broadly classified as either top-down or bottom-up. In top-down methods, lithographic techniques are used to cut larger pieces of a material into nanoparticles. For instance, particle sizes smaller than 100 nm and 30 nm can be produced using extreme UV photolithography and electron beam lithography, respectively [18, 35].

According to Govender [36], certain biological organisms that are referred to as *prokaryotic* and *eukaryotic* organisms - as well as several fungal species - produce metal oxide nanomaterials when exposed to solutions that comprise the metal salt. The physico-chemical properties of each nanoparticle vary considerably. However, based on the universal agreements as highlighted by Li et al. [37], there are a number of properties that nanoparticles should have to be considered fit for specific applications or at least with due warnings of their toxicological impact in applications. Properties like chemical composition, mass, particle number and concentration, surface area concentration, size distribution, specific surface area, surface charge potential, stability [21, 26], solubility, depend on the nature of the nanoparticle shell. Properties like solubility, transparency, color, conductivity, melting point and catalytic behavior mainly depend on the actual particle sizes. Similarly, surface composition of the nanoparticles affects the dispersability, optical properties, conductivity and catalytic behavior of the particle [16, 38]. Even though nanoparticles play a vital role in the development of new technology, there are still limitations and unsolved challenges. For instance, because nanoparticles have large surface area and extremely small particles size, it is difficult to work with them in both liquid and dry form because of particle-particle aggregation [39].

ZnO is one of the most studied of the engineered metal oxide nanoparticles. It is an inorganic semiconducting material that is a very versatile and important [40]. Due to its unique nanoscale properties, it finds application in many applications such as laser diodes, solar cells, gas sensors, optoelectronic devices and others [41].

1.2 The research question

According to statistics shown by the research database, SCOPUS [42], ZnO is the most synthesized and studied nanomaterial. The statistics are summarized in Figure 1.5. Presently, researchers rely on the expensive techniques mentioned above. These methods require good vacuum, high temperature, and it involve complex processes. They are corrosive and generally involve toxic gasses.

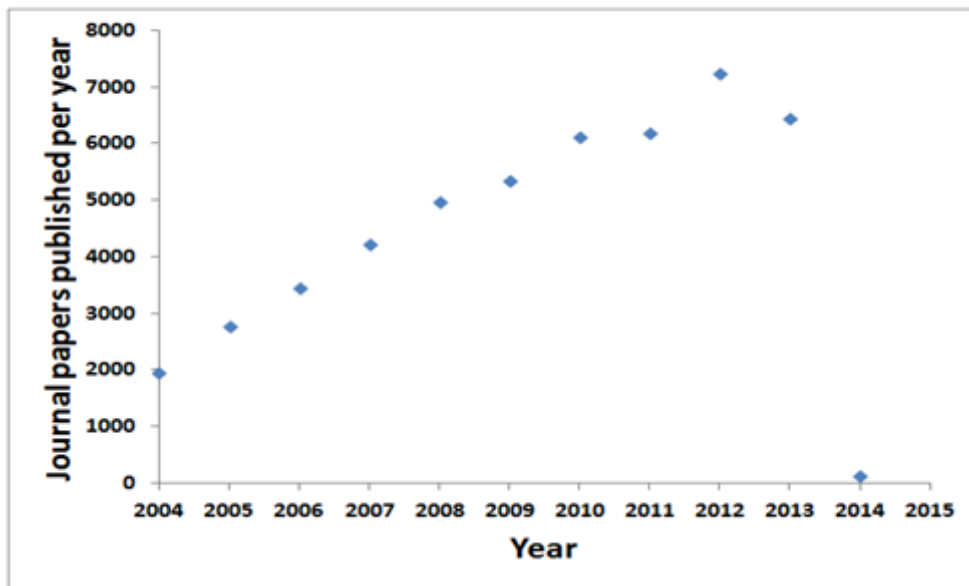


Figure 1.5: The number of ZnO-related research papers published between 2004 to 2014 [42]

In this work the zinc-air (ZAC) system is investigated as a feasible and cheaper alternative to produce ZnO nanoparticles. We investigate the scope of the method from the basic theory, to the estimation of yield, surface effects and actual resulting particle sizes. By utilizing this system, we can possibly also find alternative ways of improving the existing primary batteries as well and thus provide cheap, high performance zinc-air batteries for a multitude of applications. Therefore, the study has the potential to expand current knowledge regarding synthesis alternatives as well as to provide a

route to improve existing zinc-based power sources by identifying products that improve cell performance.

1.2.1 Aims and objectives

This project was conducted to evaluate the fabrication of ZnO nanostructures using the ZAC system method and assess the method's potential for the reliable synthesis of ZnO nanoparticles. The objectives of this study are:

1. To prepare ZnO nanoparticles by a zinc air system, the main considerations being availability, low cost and environmental impact of the components.
2. To investigate the effect of electrolyte concentration and annealing temperature on particle size by SEM techniques.
3. To characterize the crystal structure and particle size using XRD techniques.
4. To investigate the surface morphology of the zinc electrode using SEM.
5. To study the elemental and chemical composition using EDS.
6. To study the optical properties using UV-Vis spectroscopy
7. To investigate potential yield of the method.

1.3 Outline of the dissertation

Chapter 1 introduces the concept of nanoparticles and explores their potential applications. The chapter also defines the research question and outlines the specific objectives while stating the main research hypothesis.

Chapter 2 provides background information on ZnO nanoparticles and the properties that make ZnO nanoparticles a potential candidate as well as existing

synthesis methods for ZnO nanoparticles.

Chapter 3 provides an overview of the ZAC system design and construction. The chapter also proposes a method to electrically characterize the ZAC system. Furthermore, Chapter 3 provides a detailed introduction to characterization for the surface, morphological and optical properties of the ZAC cell products using standardized techniques.

Chapter 4 investigates the effects of electrolyte concentration on the surface, morphological and optical characterization of the nanoparticles obtained using the ZAC cell.

Chapter 5 discusses the effects of annealing on the surface, morphological and optical characterization of the nanoparticles obtained using the ZAC cell.

Chapter 6 makes concluding remarks and suggest directions for possible future studies.

Chapter 2

A Review of the Literature

2.1 Background of zinc oxide nanoparticles

Over the last two decades, different methods have been employed to synthesize the different nanostructures as mentioned above. These methods help to understand the meso-physics of growing nanomaterials. ZnO is one of the mostly studied metal oxides. It generally appears as a white crystalline powder and is regarded as an inorganic semiconducting material that rarely occurs in nature. It is a very versatile and important material that is insoluble in water and in alcohol [40, 43]. ZnO is generally observed as a “white powder” and is commonly known as zinc white. Sometimes it appears yellow to reddish in color due to the presence of manganese and or other impurities. The crystal structure of zinc oxide is said to be thermo-chromic, which means that it has the ability to change color when exposed to different temperatures. For instance, when ZnO nanomaterial is heated it changes from its original white to yellow due to the loss of oxygen. When it is cooled it changes back to white due to the gain of oxygen. Table 2.1 shows some physical properties of ZnO at ambient temperature and pressure. ZnO can be composed of different growth morphologies such as nanorods, nanocombs, nanowires, nanosprings and nanocages [44].

Table 2.1: Some physical properties of ZnO at ambient temperature and pressure.

<u>Property</u>	<u>Value</u>
Molecular formula	ZnO
Molecular Weight	81.37
Relative Density	5.607
Melting Point	Zinc oxide sublimes at atmospheric pressure at temperatures over 1200°C Under high pressure a melting point of 1975°C has been estimated
Saturated vapor Pressure (1500°C)	12mm Hg of mercury
Refractive Index	w = 2.004, e = 2.020
Heat of sublimation between 1350°C and 1500°C	539.7 kJol/mol (vapor not disassociated) and 40.25 kJol/mol (vapor associated)
Heat Capacity	Cp = 9.62 cal/deg/mole at 25°C
Coefficient of Thermal Expansion	4 x 10 ⁻⁶ /°C
Color/appearance	White solid powder

2.1.1 Crystal and surface structure of ZnO

There are three known molecular structures of ZnO. These are cubic zinc blende, hexagonal wurtzite and rock salt (see Figure 2.1 and 2.2). Zinc blende structure consists of two main atom types forming cubic lattices. It is different from rock-salt structure as the two lattices are positioned relative to one another. The zinc blende structure has a tetrahedral coordination. Each atom is connected to four atoms of the opposite type, positioned like four vertices of a regular tetrahedron. Altogether, the arrangement of atoms in zinc blende

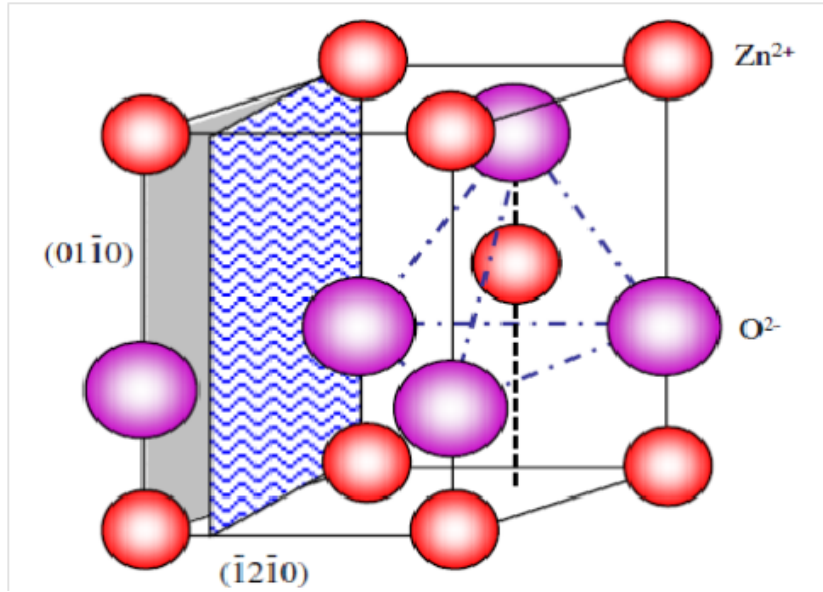


Figure 2.1: Wurtzite structure model of ZnO. The tetrahedral coordination of Zn-O is shown. Wang [44]

structure is the same as diamond cubic structure, but with alternating types of atoms at the different lattice sites as shown in Figure 2.2.

Hexagonal wurtzite is regarded as the most stable and common structure at ambient temperature and pressure [43]. The ideal wurtzite ZnO has a hexagonal close-packed structure with lattice parameters, $a = 0.325$ nm and $c = 0.52069$ nm and belongs to space group of P63mc [43–48]. The structure of ZnO is characterized by Zn^{2+} and O^{2-} sub lattices and because of the surrounding cations. The structure is classified as tetrahedral and stacked along the c -axis on an alternate basis as shown in Figure 2.1. The dipole moment and instant polarizations form when the two sub lattices (Zn^{2+} and O^{2-}) interacts results in a diversification of surface energy [41]. The lattice symmetry and tetrahedral coordination in ZnO results in pyro-electricity in hexagonal ZnO and piezoelectricity of the zinc blend ZnO [43]. The tetrahedral coordination in ZnO results not only in non-central symmetric structure with polar symmetry but also plays a crucial role in growth, defect generation and

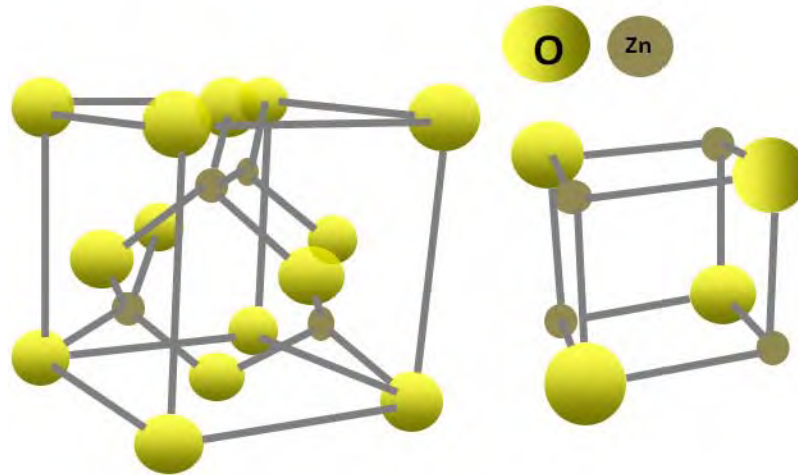


Figure 2.2: The zincblende (left) and rock salt (right) phases of ZnO.

etching of ZnO [21]. Many researchers have been involved in investigating the piezoelectric property of ZnO nanostructures for their potential applications in nano-electromechanical systems [45, 46].

In non-central symmetric structures due to external pressure that induces lattice distortion might result in a displacement of positive and negative centers which leads to a local dipole moment that can be observed over the crystal structure [43]. Based on tetrahedral bonded semiconductor materials, ZnO shows the highest piezoelectric tensor which provides a large electro-mechanical coupling [49]. Due to the pyro-electricity and piezoelectricity, zinc and oxygen planes bear electric charge. However, the electrical neutrality is maintained mostly in relative materials when zinc and oxygen planes reconstruct at atomic level. This effect is not seen in ZnO^- (0001) because the surface is relatively flat, more stable and without reconstruction [7, 50, 51].

Regardless of the above-mentioned of the ZnO structures, wurtzite ZnO has four common surfaces, the polar Zn (0001) and O (000 $\bar{1}$) terminated faces and the non-polar (00 $\bar{2}$ 0) and (00 $\bar{1}$ 0) faces. The polar surface of ZnO that is formed by oppositely charged ions produced by Z^+ (0001) and O^- (000 $\bar{1}$) is also the

most basic characteristic of ZnO. This stable polar surface results in the unique spontaneous polarization that is observed in ZnO. Polar charge interaction depends on charge distribution over the surface as shown in Figure 2.3. This can be explained by the arrangement of ZnO structure, where the structure is arranged to minimize the electrostatic energy with the stacking sequence AaBbAa along the c-axis. However, most of the well-known structures arise from this factor [44, 52, 53]. In general, in order to maintain a stable structure, the polar surfaces must show a massive surface reconstruction.

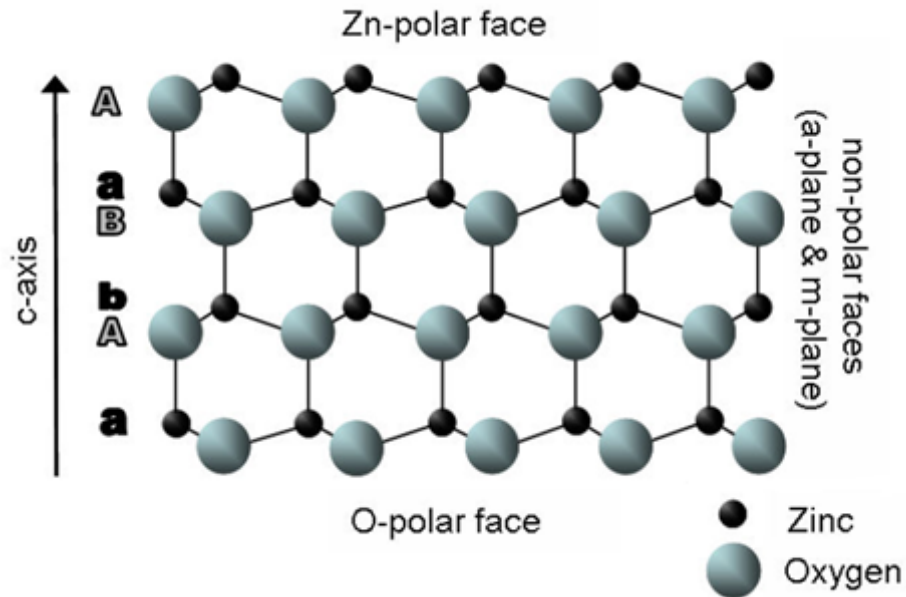


Figure 2.3: Distribution of polar charges over the surface with the sequencing arrangement of AaBbAa in c-axis

2.1.2 Electronic properties of ZnO

At ambient temperature and pressure, zinc oxide is a wide, direct band gap semiconductor of 3.37 eV and excitation binding energy of 60 me [4, 23, 47]. The large band gap gives ZnO the advantages of higher voltage breakdown, reduce electronic noise, ability to sustain large electric fields and higher power

operation than smaller bandgap materials [31]. Depending on the doping material, its band gap can be tuned from 3 to 4 eV. The wide band gap and large exciton binding energy of ZnO also make it a potential candidate to be applied in chemical sensors, luminescence devices and solar cells. Due to the presence of vacancies and interstitial defects ZnO is said to be n-type semiconductor [31,43,49]. Presently, it is still lacking a stable and reproducible p-type doping. According to Behera [43], unintentional substitutional hydrogen impurities plays a major role in explaining the n-type character shown by ZnO. However it is easy to control n-type doping by easily substituting Zn with group 3 elements such as Al and Ga, but creation of an authentic p-type doping of ZnO is still a difficult task, due to the low stability shown by p-type dopants and the abundance of n-type impurities in ZnO [41]. It is expected that creating a p-type doped ZnO would be a major breakthrough for creating nano-electronic and nano-optoelectronics. For instance, p-type and n-type ZnO nanowires may be crucial in fabricating p-n junctions, light emitting devices (LEDs) and complementary logic circuits that have application in all branches of electronics.

2.1.3 Optical properties of ZnO

The study of optical properties particularly for ZnO has been carried out over the past few decades [54–56]. To date ZnO has drawn much attention based on its unique and promising properties that makes it a promising candidate for short wavelength photonics. These properties arise from its direct wide band gap of 3.37 eV which corresponds to the energy of 3655 Å photons. ZnO is a material that strongly absorbs ultra violet light below 3655 Å and is transparent to visible wavelength of the electromagnetic spectrum [4, 57]. Zinc oxide generally appears as white in the range of visible wavelengths with

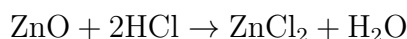
a typical refractive index of $n_w = 2.008$. But due to unintentional doping of the grown crystals ZnO crystals usually appears as red, green or yellow colored [58]. Under ultra violet (UV) light ZnO becomes photo-conductive. By the combination of optical and semiconductor properties, doped zinc oxide becomes a contender for a new generation of devices [21]. Doped zinc oxide is a promising material in solar cells because solar cells require transparent conductive coating for greater quantum efficiency. According to Yang et al. [21], both intrinsic and extrinsic effects are the contribution of optical properties in semiconductor. Intrinsic optical transition is described as the transition between the holes in valence band and electrons in conduction band where also an excitonic effect is concluded as the result of coulomb interaction [49]. The electronic states are created in the band gap when the impurities and complexes are added and influence optical absorption and emission processes. These kinds of properties can be related to extrinsic properties. Bound excitons are generally defined as an excitons that can be bound to charged donors and acceptors [4]. The electronic state of these bound excitons are highly dependent on the band structure of the semiconductor material. For example, in a shallow neutral donor bound exciton electrons are assumed to be paired off into “two-electron” state with zero spin. The additional hole is then weakly bound in the net hole-attractive Coulomb potential set up by this bound two-electron aggregate. Similarly, neutral shallow acceptor bound excitons are expected to have a two-hole state derived from the topmost valence band and a one electron interaction [23]. Due to the electron transition between the valence band and the conduction band, the ZnO nanostructures have been a promising candidate in implementing photonic devices [57]. Photoluminescence (PL) spectra of ZnO nanostructures have been previously reported. The PL spectra of ZnO nanorods show excitonic

emissions [59]. The emission peak that is clearly observed around 380 nm is due to band-to-band transition and green-yellow emission band related to oxygen vacancy are observed. According to Beheraa [57] and Fan et al. [49], quantum confinement plays an important role in enhancing the exciton binding energy. It is interesting that the observed green wavelength emission intensity increases with a decrease in the diameter of the nanowires. This is because nanowires have large surface to volume ratios. This favors a higher level of defect formation and surface recombination. The observed results are coherent with those of bulk ZnO material [41]. The double ionized oxygen vacancies have been previously reported as key attributes for red wavelength luminescence [41,49,57]. ZnO nanowires thus show good UV emission properties, while its UV lasing property is of greater significance and interest. ZnO nanowires and nanorods also have a refractive index of around 2. Their near-cylindrical geometry, makes them potential candidates for optical waveguides. It has been recently reported that ZnO nanowires can be used as sub-wavelength optical wave guides. Optically-pumped light emission was guided by ZnO nanowires and coupled into SnO₂ nano-ribbon. Based on these findings, ZnO nanostructures show promise as potential candidates for integrated optoelectronic circuits [21]. According to Hassan et al. [60], ZnO nanowires can also be utilized for polarized UV photo-detection and optical switching. This is due to the defect states that are related to wavelength.

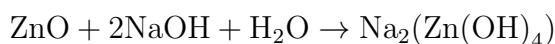
2.1.4 Chemical properties of ZnO

ZnO generally occurs as a white powder known as mineral zincite or zinc white. This mineral usually contain some manganese particles or other elements thus making it red or yellow in color [9]. When heated crystalline zinc oxide changes its color from white to yellow due to the loss of oxygen. Upon cooling it turns

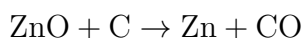
back into its original color by regaining oxygen. This is due to a very small loss of oxygen at high temperatures to form the non-stoichiometric $Zn_{1+x}O$, where at 800 °C, $x= 0.00007$. ZnO is an amphophtic semiconductor oxide that is insoluble in water and alcohol, but soluble in degrading acids such as hydrochloric acid (HCl):



When reacted with phosphoric acid, it forms a cement-like zinc phosphate cements. Since ZnO is in powder form bases can also degrade it into soluble zincates:



At about 1975 °C ZnO sublimes as Zn vapour and oxygen. In the presence of carbon, it changes to form a volatile Zn.



2.2 Methods of synthesizing ZnO nanoparticles

To date there are different methods of synthesis that are employed to synthesize this nanomaterials. The prescribed methods they follow mainly two methods namely top down and bottom up as shown in Figure 2.4. In top-down approach large system is broken down into desired compositional sub-systems, approach begins with larger starting materials and gradual controlled removed of until the desired structured is achieved. The bottom-up approach involves the fabrications of desired structure system using small systems. It begins with smaller subunits that are assembled, again with varying levels of control, depending on technique into the final product. Attrition or milling is a typical

top-down method in making nanoparticles, whereas the colloidal dispersion is an example of bottom-up approach in a synthesis of nanoparticles [61–63].

By employing these two methods one can achieve one of the four dimensions of a nanomaterials. There are zero-dimensional (0D), one-dimensional (1D), two-dimensional (2D) and three dimension (3D). 0D these are materials in which nanoparticles are isolated from each other. e.g. nanoparticles, nanoclusters, nanocrystals and quantum dots [64]. 1D nanomaterials are nanofibers and nanotubular materials with fibre length from 100 nm to tens of microns e.g. nanotubes. 2D is a single layer material, with thicknesses below 100 nm and lengths and widths that exceed nanometer dimensions e.g. thin films, graphene/graphene oxide sheets, quantum wells, 2-D electron gas and self-assembled monolayers. They have also been widely used for optical coatings, corrosion protection and semiconductor thin-film devices [65]. 3D nanomaterials are formed from two or more materials with very distinctive properties that act synergistically to create properties that cannot be achieved by a single material alone e.g. complex systems, composites, zeolites, mesoporous materials [66].

These methods each have advantages and disadvantages. The top-down method involves the thermal treatment of larger particles, and volatilization of a solid followed by condensation of the volatilized components. In this case high temperature is required to produce nanostructures thus resulting in higher production cost. In the case of volatilization of solids expensive masks are required which are time consuming when manufacturing. However, bottom up in this case is preferable because nanostructures are fabricated at low temperatures. In the bottom-up method, the fabrication of nanostructures requires the condensation of atom or molecules in the gas phase thus an expensive closed chamber containing a gaseous environment is required. The bottom up is a more convenient method to engineer nanoparticles (ENPs) [68],

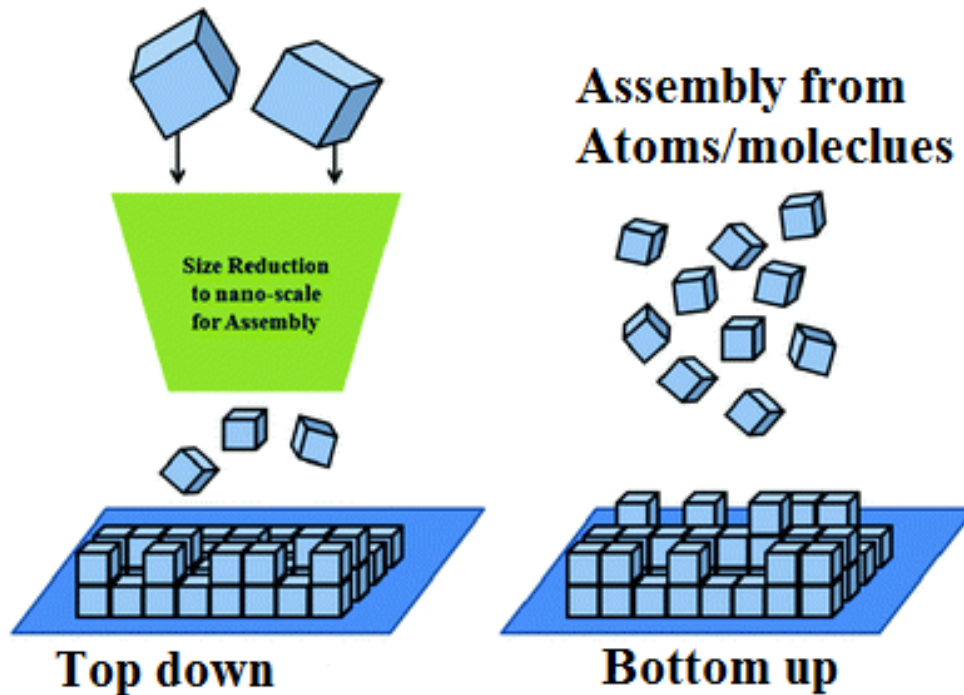


Figure 2.4: Top-down and bottom-up approaches in nanotechnology [67]

supports a better opportunity to obtain nanostructures with fewer defects, more homogenous chemical composition with better short and long range ordering and also relevant to the chemical industry. The fabrication of size of nanoparticles varies with their synthesis methods, as discussed below.

2.2.1 Vapor Transport Synthesis (VTS)

VTS is one of the commonly employed methods to synthesize ZnO nanostructures. In this process Zn and oxygen are mixed using a oxygen mixture method, this allows a oxygen to react with Zn to form ZnO nanostructures. This is however achieved by heating up Zn powder under oxygen flow and then transported and condensed onto the substrates [69, 70]. This is not a complex technique to synthesize ZnO but it is an expensive technique that requires high growing temperatures, where as high temperature environment may cause decomposition and undesired reactions in the reactor.

2.2.2 Sol-Gel method (SG)

This is a wet chemical methods that is used to fabricate metal oxides from chemical solution that acts as the precursor for an integrated network (gel) of discrete particles [71]. The precursor solution can be either deposited on the substrate to form a film, cast into a suitable container with the desired shape, or used to synthesize powders.

2.2.3 Pulsed laser deposition (PLD)

Pulsed laser deposition (PLD) is a synthetic method that utilizes a pulse laser to deposit a materials on the a substrate surface as a film. By far this method is known by producing good ZnO nanostructures with outstanding electronic and optical properties [72, 73]. The process of deposition involved in this method take place in an ultra high vacuum with the presence of gasses such as oxygen.

2.2.4 Chemical bath deposition (CBD)

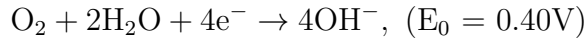
CBD is one of the commonly employed method to synthesize metal oxide as a compound semiconductors from aqueous solutions [74]. This method is commonly employed because it does not require high voltage equipment, works at room temperature, and hence it is inexpensive. With the proper controllable kinetics of formation of solids, CBD techniques can produce solid films on a suitable substrate.

However, there are complications associated with these techniques such as the need for a good working vacuum, high working temperature, the inherent process complexity, corrosiveness and the release of toxic gasses. All these lead to elevated experimental and safeguard costs.

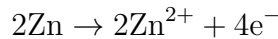
2.2.5 The zinc-air system (ZACs)

The ZACs consists of a zinc plate as the anode, sodium hydroxide (NaOH) or potassium hydroxide (KOH) and or lithium hydroxide (LiOH) as the alkaline electrolyte and oxygen as the cathode [75]. Electrolytes differ by more than just their ionic conductivity, KOH is thought to be preferable to NaOH, because K^+ has a larger ion radius and thus a lower probability of incorporation into the ZnO lattice. The oxygen that is used in this system is derived directly from the air. Moreover, the use of oxygen from the air curtail the experimental cost and make it an environmental friendly system, the operation of zinc air system is described as follows: Zinc loses electrons to an anode current collector turning to a Zn^{2+} cation. The electrons generated on the anode travel via an external circuit to an air cathode where the reduction of oxygen takes place forming hydroxyl ions (OH^-). The hydroxyl ions travel towards the anode side via the electrolyte and combine with zinc cations to form zinc oxides. The chemical reactions of Zn-air system can be described as follows:

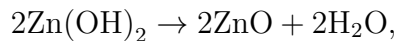
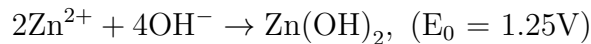
At the cathode:



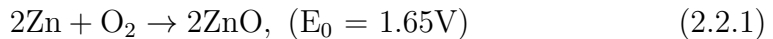
At the anode:



E_0 represents the standard half-cell electrode potential with respect to Standard Hydrogen Electrode (SHE).



The overall cell reaction can be written as follow:



From the above equations, it shows that the operation of ZAC system largely depends on the activities of reduction and oxidation reaction at air electrode and Zinc anode, respectively. In spite of the experimental simpleness, there are complicated task involved such as to understand mechanism of decomposition process, the overall formation of hydroxide ions that leads to the formation of ZnO on the zinc plate. This is because the zinc ion are more attracted to OH than H₂O. To control the formation of ZnO nanoparticles including shape there are variety of parameters that should be controlled. These includes the concentration and type of electrolyte, dimensions of the casing, exposed surface of zinc plate, air cathode dimensions and the designing of the constant current grainer.

2.2.6 Role of separator and electrolyte

The separator plays an important role in zinc air system by transporting hydroxyl ions in electrolyte from the air electrode to zinc anode electrode [76]. Thus suitable separator must be carefully chosen in order to serve this purpose. Firstly a separator must be stable in the electrolyte with suitable pore size [77], high ion conductivity [78] and insulating to electron transportation. The zincate ion must be prevented from migrating from anode to cathode thus a separator must have moderate or fine porosity. However, the concentration of electrolyte also play a vital role in formation of ZnO nanostructures, therefore it is important to find the concentration that gives the optimum cell performance. Higher the concentration of electrolyte results in high viscosity thus increase the formation of ZnO nanostructures but it also reduce the internal resistance. Moreover, it is important to remark that the electrolyte does not form part of the reaction but only takes part in the conduction of OH⁻ ions.

Chapter 3

Construction and characterization of products

This chapter presents an overview of the experimental methods starting from the design of the zinc air cell system (ZACs) and then the procedures used to synthesize ZnO nanostructures on a zinc-plate. The characterization methods used are divided into two categories, namely electrical methods and standardized methods.

3.1 Fabrication of the ZACs

One of the objectives of this research was to use simple apparatus and methods to synthesize ZnO nanostructures. However, this was achieved by utilization of commercial wire sponge or steel wool (purchased at Shoprite), a porous void fill recycled paper, recycled zinc plates extracted from Eveready transistor batteries purchased at Shoprite and further cleaning was done. A clear, perspex box with certain dimensions was used as a casing and commercial sodium hydroxide pellets CP from Associated Chemical Enterprises (PTY) LTD and also distilled water. Set of zinc plates were cut into 70 mm x 50 mm in dimensions and cleaned with wire sponge (steel wool) until the plate appears shinny as shown in Figure 3.1.

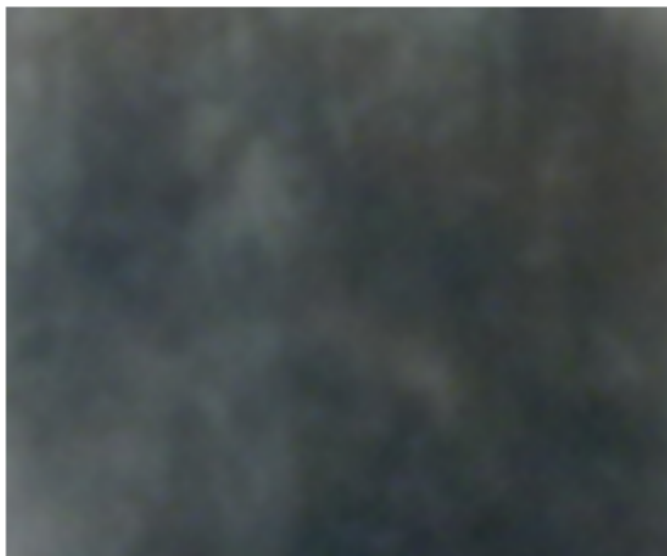


Figure 3.1: Zinc plate after washing

Copper wire was crimped onto each plate to allow external connection to the zinc anode. Commercial steel wool with the mass of 5g was used as the positive cathode. A length of copper wire was also crimped on steel wire to allow external connection to the cathode. A porous, packaging void-fill recycled paper was used to prevent a short circuit between electrodes and to allow the flow of oxygen. The zinc-plate, steel wool and void-fill paper were placed inside a clear, perspex box with the dimensions of 108 mm length, 64 mm wide and 30.4 mm width as shown in Figure 3.2. Figure 3.2 shows the final design of ZACs after different designs were used to optimize the growth conditions. The electrolyte was then injected on the casing to allow the transfer of electrons from the anode to the cathode. The oxygen from the air diffuses into the cell and it becomes the cathode reactant. The presence of the air cathode allows the reaction of oxygen and aqueous NaOH electrolyte to take place. When oxygen diffuses into the electrolyte hydroxyl ions (OH^-) are formed. These ions travel through the electrolyte into the zinc anode and form zinc oxide, and the chemical reactions described by Equations (2.2.5) to

(3.3.1) occur.

3.1.1 The electrolyte solution

Solutions of pure sodium hydroxide of 0.4M to 2M concentration were prepared in distilled water using commercial sodium hydroxide pellets CP from Associated Chemical Enterprises (PTY) LTD and distilled water. This was done by dissolving 2, 4, 6 and 8 g of NaOH respectively in 100 ml distilled water under constant magnetic stirring at room temperature to ensure a homogeneously mixed solution. Then the solutions were then cooled to room temperature before being injected into the cell enclosure, Figure 3.2 to allow the transfer of electrons from the anode to the cathode following the process described in chapter 3.

3.2 Proposed method for ZAC electrical characterization

Two multimeters were employed to evaluate the room temperature open-circuit voltage (V_{OC}) and the constant-load, closed-circuit voltage (V_{cc}) performance of the ZACs. The internal resistance (R_{th}), current output (I) and power (P) parameters were indirectly deduced from the knowledge of (V_{OC}), (V_{cc}) and the constant load. The performance of the ZAC was then taken as the behavior of (V_{OC}), (V_{cc}), (R_{th}), I and P as functions of time. The closed-circuit cell load was a $470\Omega/0.25$ watt standard resistor. The cell current was measured over a discharge time of 1 hour. The experiment was repeated for the five cells with the concentrations above. In order to measure V_{OC} the voltmeter was connected across point A-B in Figure 3.3. The current flowing through (R_{th})

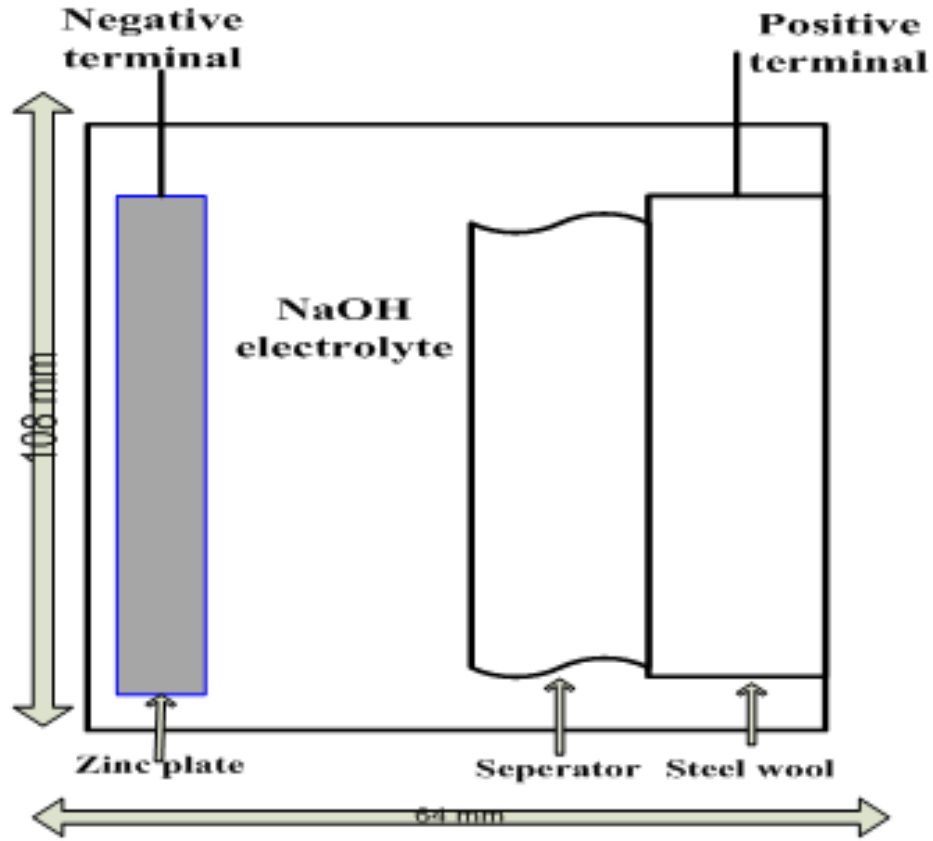


Figure 3.2: Schematic diagram of the apparatus used to synthesize ZnO nanostructures by ZACs

is described using Thevenin's theorem by:

$$I_{ss} = V_{oc}/R_{th} \quad (3.2.1)$$

Where V_{oc} is the open circuit voltage at the terminals, I_{ss} is current flowing through the circuit and R_{th} is the input or equivalent resistance at the terminals when the independent source are turned off. We are proposing this unique approach using standard network theory because of the following. The infinitesimal power in a load across which a voltage drop dV is developed when a constant current I flows is given by

$$dP = IdV \quad (3.2.2)$$

The change in energy delivered to the load i.e actual work done in the load over the time interval dt is then

$$dE = dPdt \quad (3.2.3)$$

Assuming that the cell output is reasonably steady, the infinitesimal work done is

$$dE = Pdt \quad (3.2.4)$$

The total energy of the cell is therefore given by

$$E = \int dE \quad (3.2.5)$$

which represents the area under the power-versus time, for example in Figure 3.7. This approach allows the determination of the energy delivery capacity of the cell for a specific purpose.

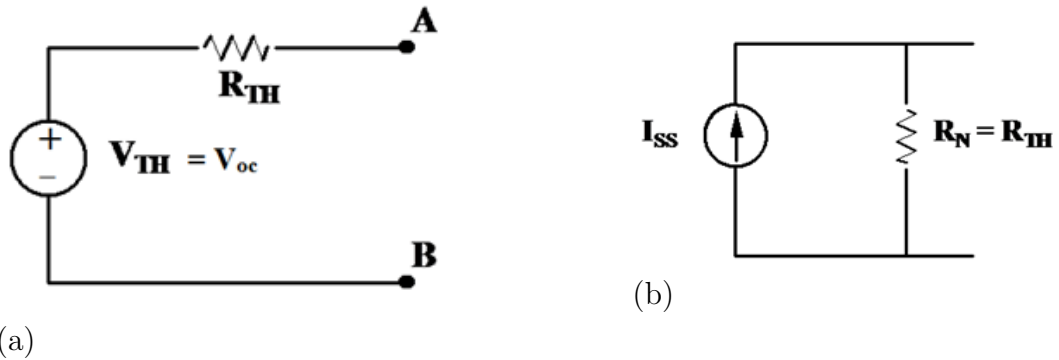


Figure 3.3: Circuit illustrations of thevenin's (a) and Norton's (b) theorems

3.2.1 Open-circuit voltage characterization

Zinc air cell/batteries have a theoretical and practical open-circuit voltages V_{OC} of 1.65V and 1.2V respectively [77]. In this investigation the V_{OC} was monitored for 12 hours at room temperature and it was found to be steady at around 1.2V as shown in Figure 3.4. The values obtained are in agreement

with Yap et al. [8] but slightly lower than those reported by Mohamad [77]. This is due to the use of different electrolytes used. The specific electrolytes differ on account of different ion conductivity.

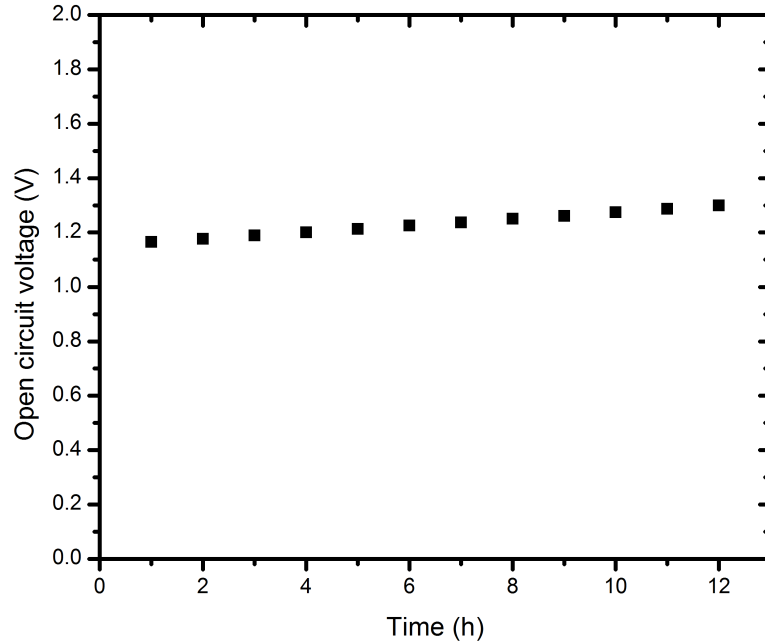


Figure 3.4: Twelve-hour measurements for open circuit voltage of ZACs

3.2.2 Closed-circuit voltage characterization of ZAC

The closed-circuit voltage (V_{OC}) versus time performance of the constructed ZACs with concentrations of 0.4, 0.5, 0.6, 1 and 2M over one hour is shown in Figure 3.5. From the graph, 0.5 and 1M can sustain a load of 470 ohm for longer time compared to cells with 0.4, 0.6, 1 and 2M. The basis of this is the cell voltage that remaining constant within 10% of 0.85V. The measured voltage drops as results on an increase in internal resistance are shown in Figure 3.6. Figure 3.7 shows the output power of the cell as a function of time. The internal resistance of the cell was measured and it is

shown that the resistance of the cell is depends directly on the electrolyte concentration. However, at concentrations of 0.4, 0.6, 1 and 2M V_{OC} is lower and the extent of passivation as a result of increased cell internal resistance is greater. The overall effect is then poorer reactions at the cathode and the anode, leading to lower power output. Overall an electrolyte concentration of 0.5M concentration was found to be the optimal concentration for ZACs open-circuit voltage, as shown in Figure 3.8.

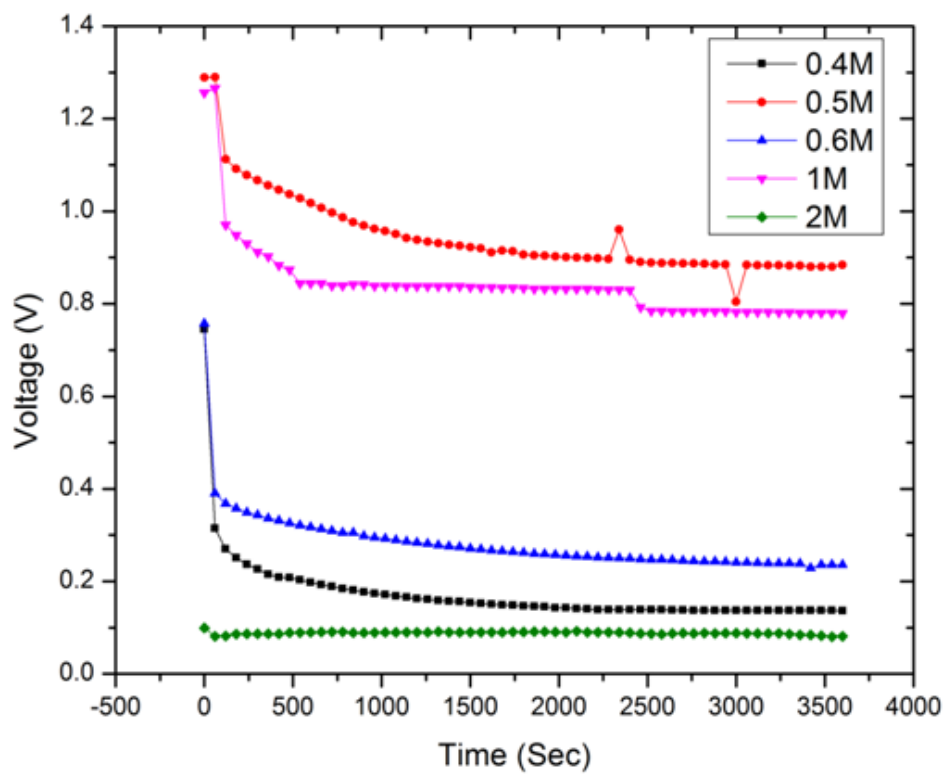


Figure 3.5: Behavior of the cell at different electrolyte concentraions

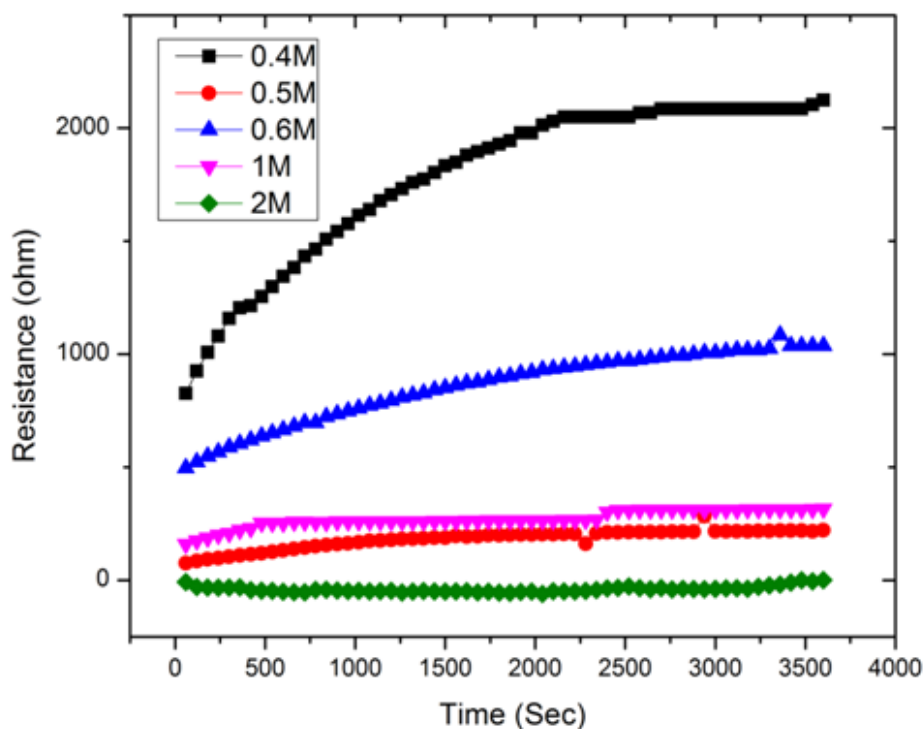


Figure 3.6: Resistance measurement

3.3 Surface, morphology and optical properties

3.3.1 An overview of standard characterization methods

Different, well-known characterization techniques were employed to study the particle morphology, elemental composition, and structure of synthesized ZnO nanoparticles. These techniques are: X-ray diffraction (XRD), scanning electron microscopy (SEM), Energy Dispersive X-ray Spectrometry (EDS) and UV-Vis Spectroscopy (UV-Vis). The theory of these characterization techniques are briefly covered in this chapter. It also gives the experimental set-up and layout of the methods used for characterization.

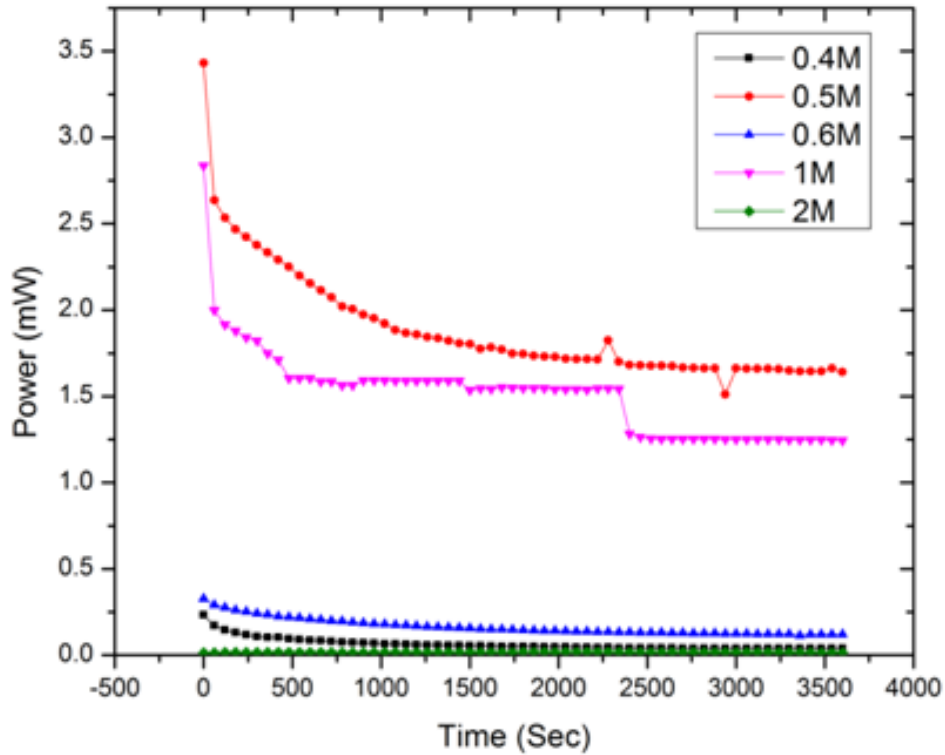


Figure 3.7: Power behavior of a cell

3.3.2 X-ray diffraction (XRD)

XRD is one of the commonly employed non-destructive techniques in determining certain parameters such as the crystal structure, composition, quality, lattice parameters, orientation, defects, stress and strain of matter in either a powder or thin film form [79]. The XRD uses X-Ray (or neutrons) beam with a specific wavelength to probe the sample in order to determine the above mentioned parameters [80]. During the analysis of XRD measurement, X-Rays are directed towards the sample specimen and proceed to elastically scatter off the electron clouds of atoms in the sample. Detector is then used to measure the X-Ray intensity as a function of the angle of a beam diffraction. A periodic structure within the sample leads to interference fringes determined by the periodic arrangement of the atoms. Thus Bragg's Law plays a crucial

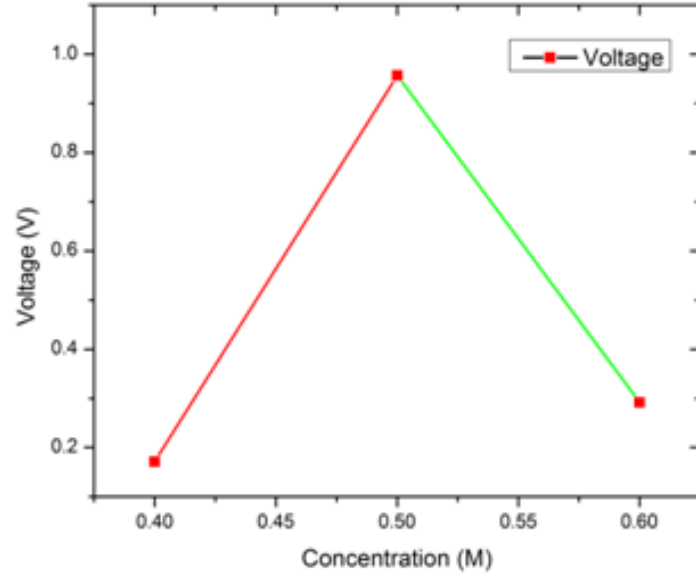


Figure 3.8: Optimum concentrations for ZAC system

role in interpretation of these peaks.

$$\lambda = 2d \sin \theta \quad (3.3.1)$$

Where d is the distance between the atomic planes, θ being the scattering angle, and λ being the wavelength of the incident X-ray radiation.

However, by knowing the widths on the diffraction lines, size, size distribution and strain of the nanocrystals can be easily determine. The lattice spacing and the crystal size of the sample is determined by using peaks position and full width half maximum (FWHM). Another alternative way of determining the crystallite size of a sample is through using Debye-Scherrer equation [109] which is given by

$$D = k\lambda/(\beta \cos \theta) \quad (3.3.2)$$

Where D is the size of the crystallites, β is the full width at half maximum of a diffraction line located at angle θ while λ is the X-ray diffraction wavelength of Cu Ka radiation (0.1514 \AA) and k is a Scherrer constant (0.94), which depends on the peak breadth, the crystallite shape, and the crystallite size distribution.

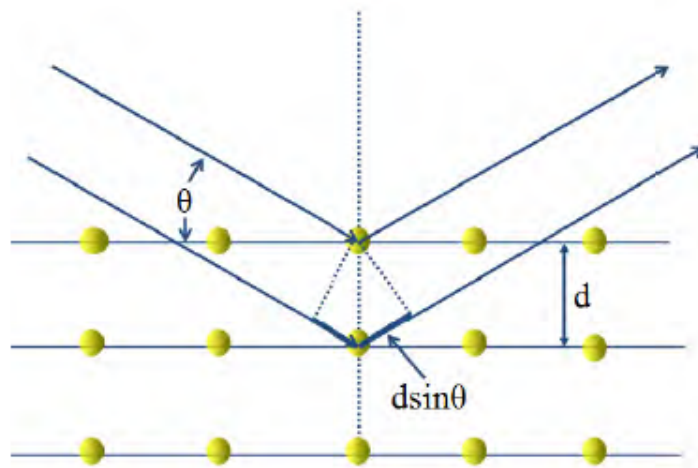


Figure 3.9: Bragg's law derivation.

Types of X-ray spectra found on XRD

When the aimed sample is bombarded with the cloud of electrons accelerated with high energy from the filament it result on two types of X-ray spectra being generated. The first type being continuous and the second type being characteristic spectra. The continuous spectra is produced when the electrons hit the targeted sample, it is characterized by the wide range of wavelengths x-rays depending on the targeted material and voltage across the X-ray tube. However, when the applied voltage is raised above a critical value, characteristic of the target metal, sharp intensity maxima appear in the spectrum. These are the 'characteristic lines' and they are produced by exciting an electron out of its shell (only K lines are used in x-ray diffraction due to absorption). The K_{α} lines are produced as an electron from one of the outer shells falling into the vacancy created in the K shell, thereby emitting energy in the process as x-rays. The characteristic spectra is produced when the electronic transition occurs amongst individual atoms of the targeted specimen as a results of high voltage. This type of spectra is defined more by Bohr model of atoms. In

this model the nucleus of the atom containing the protons and neutrons is surrounded by shells (K, L and M) of electrons. The K- Shell is surrounded by L- and M- shells. When the electrons are accelerated with high energy towards the targeted material and their energy is high enough to dislodge the inner K- shell electrons results in electronic transition. The electrons from the outer L - and M - shells move in to take the place of those dislodged. The electronic transition that occurs between L to K - shell produces K_{α} X-rays, while electronic transition that occurs between M to K- shell produces K_{β} X-rays. Figure 3.10 shows the comparison between the two spectra, the characteristic X-rays have a much higher intensity compare to continuous spectra.

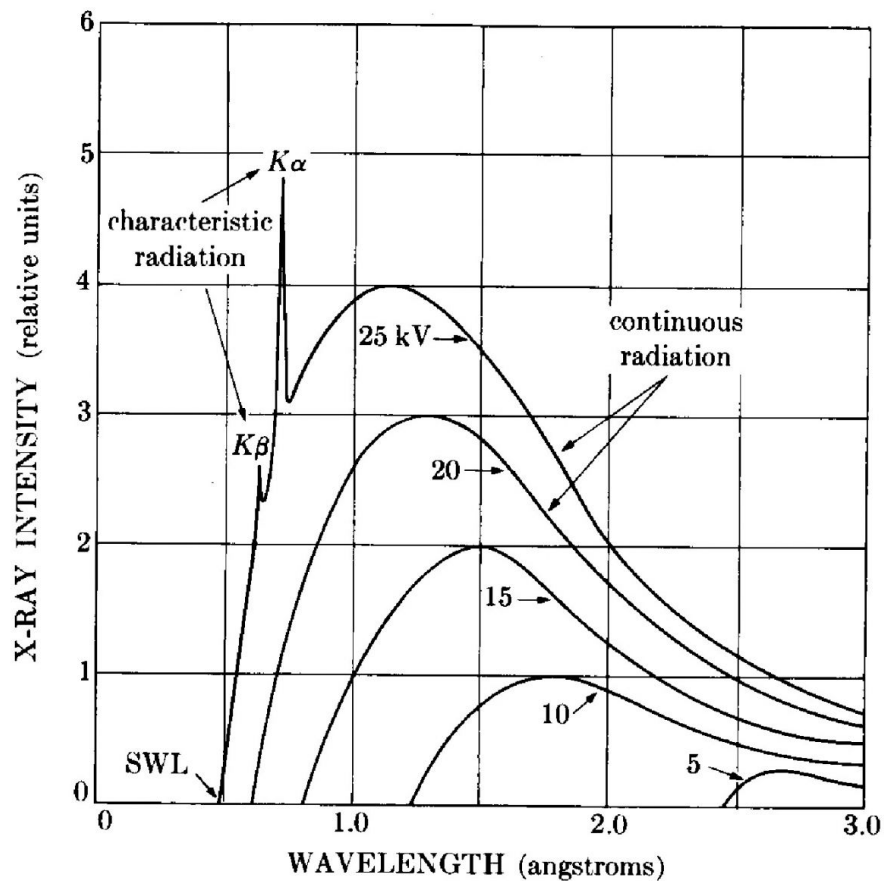


Figure 3.10: Continuous and characteristic spectra [81]

3.3.3 Scanning electron microscopy (SEM)

Scanning electron microscopy (SEM) is among the most powerful surface techniques that provides information on the specimen or substrate such as composition, topology and crystallography [82]. It is a very good technique for investigating the surface morphology of nanoparticles. SEM utilizes electron beam generated by tungsten or lanthanum hexaboride to probe a sample [83]. An electron beam is accelerated and directed using positively charged wire grids, and focused using electrostatic and magnetic field lenses. As the electron beam is systematically scanned over the sample, it results in dissipation of the electron beam energy in the near surface region of the sample thus low energy secondary electrons, backscattered electrons (BSE), Auger electrons, characteristic x-ray and continuum x-ray can be detected by electron detector. The signal from low energy secondary electrons is then used to create the image of the analyzed sample. Secondary electrons give the most valuable information about the morphology and topography of the analyzed material while backscattered electrons they provide valuable information in terms illustrating contrasts in composition in multiphase samples. X-ray generation is produced by inelastic collisions of the incident electrons with electrons in shells of atoms in the sample. As the excited electrons return to lower energy states, they yield X-rays of a fixed wavelength. Thus, characteristic X-rays are produced for each element in a sample that is “excited” by the electron beam. Depending on the instrumental aperture and resolution, the maximum magnification for a SEM can be as large as one million times, thus allowing the observation of atomic clusters and nanostructures. It should be pointed out that the image resolution given by SEM largely depends on interaction of electron probe with specimen. Figure 4.2 shows an operation of SEM from scanning of the sample up to data acquiring.

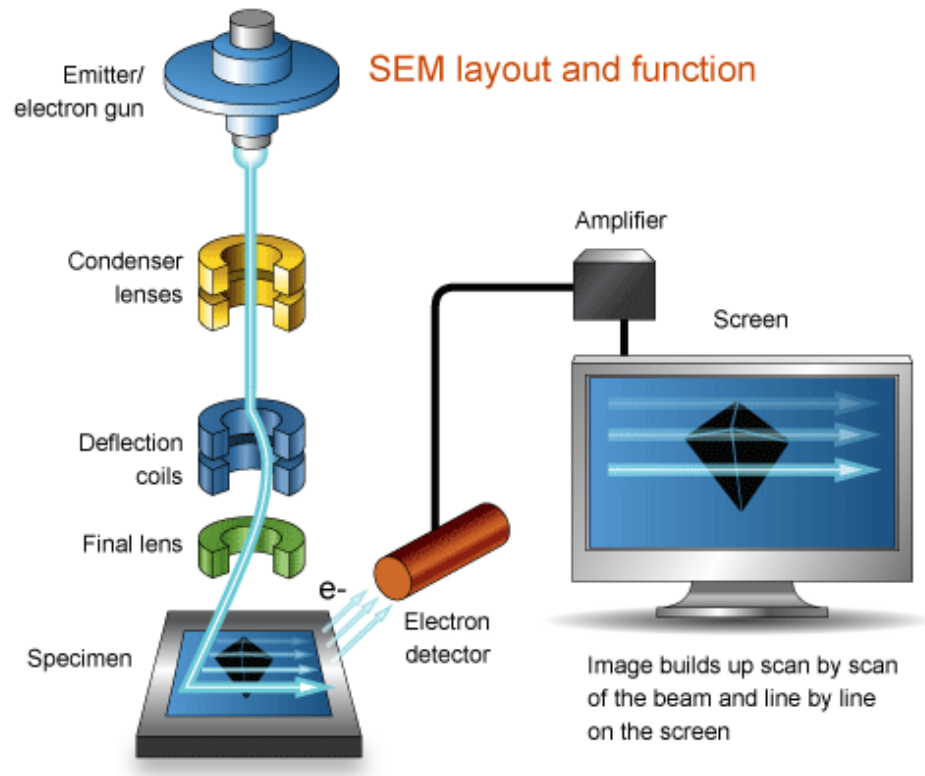


Figure 3.11: Operation of the SEM instrument. [81]

3.3.4 Energy Dispersive X-ray Spectrometry (EDS)

The EDS (or EDX) spectrometer is among the most commonly employed analytical technique in elemental analysis of the solid samples [84]. It uses a high-energy focused beam of electrons produced by thermionic sources such as a tungsten hair pin exaboride (LaB6) crystal to irradiate the solid surface in order to obtain the localized chemical analysis. Its characterization capabilities are due in large part to the fundamental principle that each element has a unique atomic structure allowing unique set of peaks on its X-ray spectrum. Based on the principle, EDS is capable of detecting all the elements present on the analyzed sample with the atomic number 4 (Be) to 92 (U) [85]. There are two analysis methods that are associated with EDS spectrometer namely, qualitative and quantitative analysis. Qualitative analysis is regarded as a first

step of analyzing an unknown sample by identifying the present elements on the obtained X-ray spectra using tables of energies or wavelengths. Quantitative involves the determination of the concentration of the elements present on the sample by measuring the intensities of each element line that appears on the X-ray spectra and compare it with a calibrated standards of know composition. In the analysis only peaks which are statistically significant should be considered for identification because the higher the peak in the spectrum, the more concentrated the element is in the specimen as shown in Figure 5.5 [86]. From a typical spectrum presented on Figure 5.5, it consist of

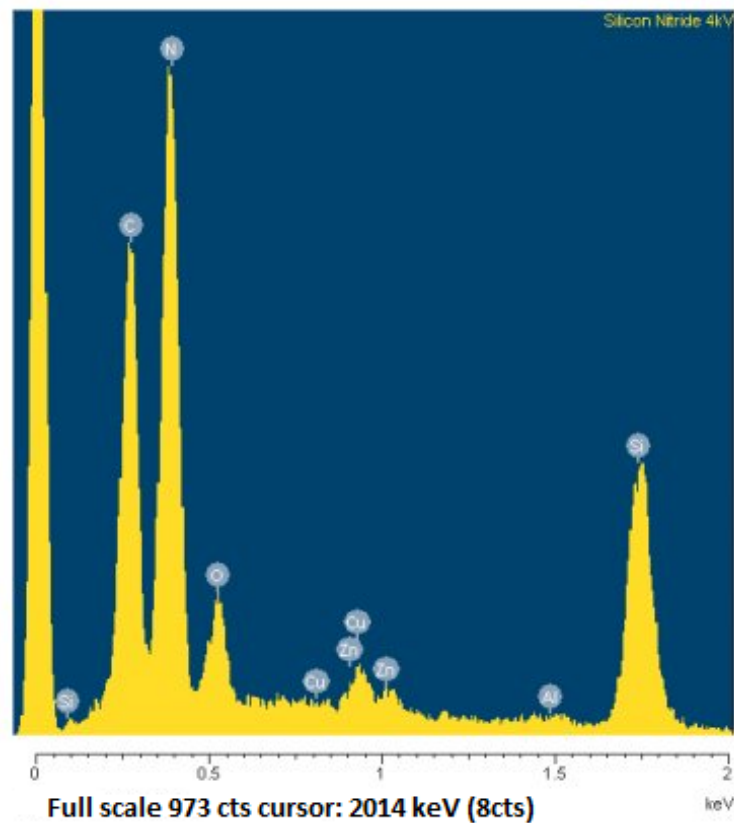


Figure 3.12: Typical EDS spectra. [86]

a number of higher peaks which are place on top of slowly varying continuous background. The background is produced by Bremsstrahlung x-rays while the higher peaks are produced by characteristics x-rays. Although the natural

energy spread of the x-rays in a particular emission line is very small, the x-ray line is recorded as a Gaussian distribution several tens of eV wide because of noise in the detector and amplifier system.

3.3.5 UV-Vis spectrometer

UV-Vis spectrometry is a non destructive technique which measures the light intensity when passes through the sample and compare it to the light intensity before it passes the sample. The principle of UV-Vis spectroscopy is based on the ability of the material to absorb ultraviolet and visible light. The relationship between the input and output intensity is described by Beer-Lambert Law:

$$e^{-A} = I/I_o \quad (3.3.3)$$

The absorbance, A , can be divided by the path length, l , to yield the absorption co-efficient α which quantifies the absorbance per metre thus taking film thickness into account. The spectroscopy consist of light source, a sample holder, a diffraction grating which separates the different wavelengths of light, and a detector. The radiation source normally a tungsten filament(300-2500nm) and a deuterium arc lamp which is continuous over the ultraviolet region (190-400 nm). The detector is typically a photodiode or a charge couple device (CCD). Photodiodes are used with monochromators, which filter the light so they only of single wavelength reaches the detector. Diffraction gratings are used with CCDs, which collects light from the different wavelengths on different pixes. The operation of UV-Vis spectrometry is shown in Figure 3.13.

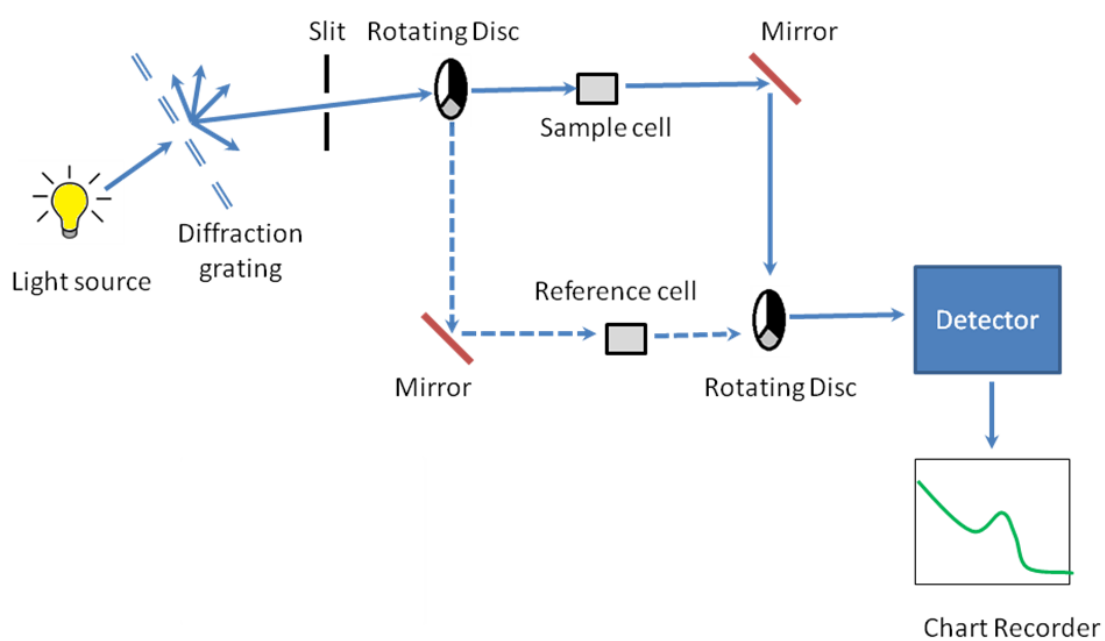


Figure 3.13: Operation of the UV-Vis instrument [87].

Chapter 4

Effects of electrolyte concentration

4.1 Introduction

ZnO is a group II-VI semiconductor compound with a wide direct-band gap of 3.37 eV [88] and an excitation binding energy of 60 meV [89]. It has three stable structures, namely cubic rocksalt, zincblende and hexagonal wurtzite (lattice parameters $a = 0.325\text{nm}$, $c = 0.521\text{nm}$) [90], [91]. The large band gap gives ZnO the advantage of higher voltage breakdown, reduced electronic noise, ability to sustain large electric fields and higher power operation [41]. With the emergence of nanotechnology, this material has been employed in a wide range of industrial applications. For instance, it finds use as a semiconductor in electronics devices and sensors, as an ingredient in cosmetics and in biomedicine [92–95].

4.2 Characterization

In this chapter, the effects of different electrolyte concentration on grown ZnO nanoneedles on a zinc plate at room temperature is presented in terms of orientation and yield using the information gathered by a Shimadzu model ZU SSX-550 SEM and TEM characterization techniques. Secondly, crystallinity

of ZnO nanoneedles is predicted using XRD technique using a Bruker D8 X-ray diffractometer operating at 40 kV and 20 mA using $\text{Cu K}\alpha = 0.15406$ nm for elemental analysis. Finally, EDS Spectrometry results reveal that the synthesized nanomaterial is ZnO.

4.2.1 Structural analysis using XRD

An XRD was employed to prove that the synthesized nanoparticles on the zinc substrate are ZnO. No characteristic peaks from impurities were observed in the samples which mean that the crystals were composed of a pure ZnO phase. All the peaks that appears on the XRD pattern as shown in Figure 4.1 are in agreement with the JCPDS card no.: 04-0831 for hexagonal structured zinc that belongs to space group P63/mmc (194) with lattice parameters of $a = 2.64 \text{ \AA}$ and $c = 4.95 \text{ \AA}$ and or JCPDS card no.: 80-0075 for hexagonal wurtzite structured space group P63mc (186) with a maximum lattice parameter $a = 3.24 \text{ \AA}$ and constant $c = 5.21 \text{ \AA}$ respectively. Figure 4.1 shows a compilation of XRD measurements of ZnO synthesized with the variation of NaOH electrolyte concentrations ranging from 0.4 to 2M. From these images, it is observed that nanoneedles start to grow on a zinc plate at 0.5M with size vary from 19 to 39nm. This is thought to be the process of effusion of atoms from the source material and these atoms rapidly lose their energy by colliding with gas atoms. The XRD measurements for samples synthesized at 0.4 and 0.5 M shows no traces of ZnO diffraction peaks but only pure zinc diffraction peaks appears with the preferred hexagonal orientation of (002) planar. The samples prepared with 0.6M, 1M and 2M shows the trademark of hexagonally wurtzite ZnO s tructure with preferred orientation (101). Other than the preferred orientation (101) planar, there are other 9 diffraction peaks that correspond to hexagonally wurtzite ZnO structure which are (100), (002),

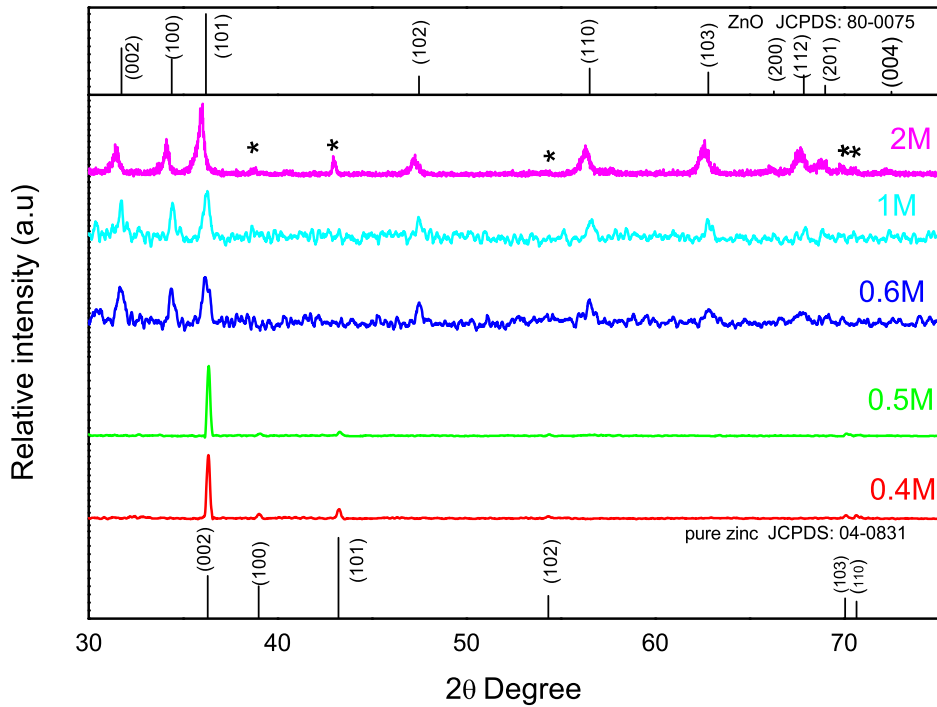


Figure 4.1: XRD patterns of the Zn anode after the synthesis at different NaOH concentrations of (a) 0.4M (b) 0.5M (c) 0.6M (d) 1M and 2M:

(102), (110), (200), (112), (201) and (004). It is also noted that as the concentration increases ZnO diffraction peaks become broad due to decrease in particle sizes. The XRD spectra show that ZnO nanoneedles grown with 0.6M, 1M and 2M are crystalline. The sample prepared with 2M shows some peaks that belong to pure zinc phase. This is attributed to the passivation of zinc plate due to high ionic conductivity. However, the XRD spectrum of ZnO nano-particles synthesized with 0.4M and 0.5M are exceptions because they do not show any preferred significant peaks of hexagonally wurtzite ZnO structure besides the preferred (002) plane, thereby showing amorphous nature [96]. SEM images of the grown ZnO are shown in Figure 4.2. The crystalline sizes, lattice parameters and lattice spacing of ZnO were then calculated

using Debye-Scherrer and Bragg's equations (3.3.2) and (3.3.1) respectively. An average lattice spacing of ≈ 0.265 nm was obtained for the synthesized ZnO nanoneedles, which can be closely correlated with the (0 0 2) interplanar spacing of ZnO Wurtzite structure reported by [97]. For the wurtzite structure the inter-planar distance of the (h k l) plane is related to the lattice parameters a and c via the Miller indices hkl.

$$(1/d_{hkl})^2 = 4/3 + ((h^2 + k^2 + hk)/a^2) + l^2/c^2, \quad (4.2.1)$$

where a and c are the lattice constants; h, k, l are Miller indices. With the approximation of the first order $n = 1$, lattice parameter a was calculated using equation (4.2.2) with (002) diffraction peak:

$$a = \lambda/(\sqrt{3} \sin \theta) \quad (4.2.2)$$

To calculate lattice constant c, diffraction peak (101) and equation (4.2.3) was used

$$c = \lambda/ \sin \theta \quad (4.2.3)$$

The application of Equations (4.2.1)-(4.2.3) to the data gives Table 4.1 for ZnO. The calculated parameters are in agreement with the lattice parameters of the bulk ZnO. The lattice constants a and c of bulk ZnO were determined as $a = 3.2498 \text{ \AA}$ and $c = 5.2066 \text{ \AA}$ [98]. The variance in the calculated lattice constants a and c are $3.17 \pm 0.01 \text{ \AA}$ and $5.25 \pm 0.03 \text{ \AA}$, respectively. This is within the bounds of known experimental measurements [99]. However, it has been reported that the lattice parameters appear to decrease with increasing in KOH electrolyte concentration [100]. This may be due to the lattice contraction resulting from the presence of dangling bonds on the surface of the ZnO films. Further work is needed to ascertain the trend with NaOH. The ions on the surface of the ZnO films are incompletely coordinated and

possess unpaired electrons. These dangling bonds (Zn^{2+} and O^{2-} ions) form an electric dipole, resulting in a parallel array of dipoles originating in the boundary layer of each particle, which lies in this surface and experiences a repulsive force.

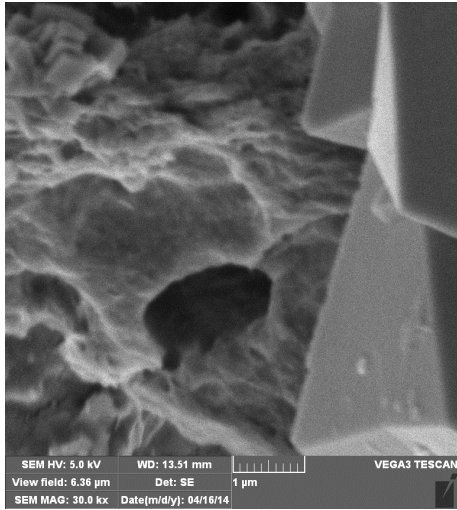
Table 4.1: Effect of electrolyte concentration on the ZnO lattice parameters.

Estimated ZnO Parameters			
Electrolyte concentration (M)	2θ (degrees)	c (\AA)	a (\AA)
0.4	36.350	5.94	2.85
0.5	36.360	4.94	2.85
0.6	34.453	5.23	3.21
1.0	34.396	5.27	3.20
2.0	34.186	5.29	3.10

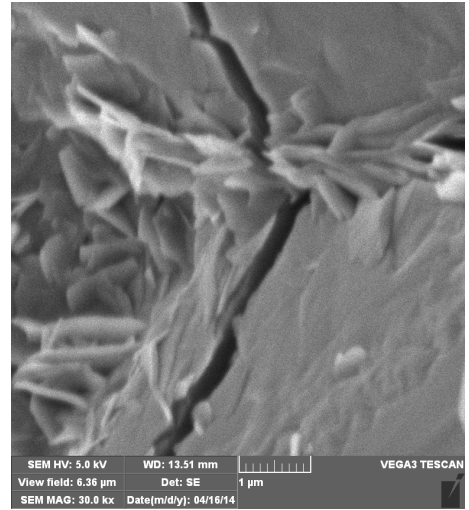
4.2.2 Surface morphology by SEM

The results of SEM are shown in Figure 4.2. It can be seen that the shape of ZnO nanoparticles grown on zinc-plate is nanoneedles with average particle size in the range of 19 to 39nm. The orientation and particle sizes of these nanoneedles are highly dependent on the electrolyte concentration. The higher the concentration, the more oriented nanoneedles become. Figure 4.2 (a) shows the rough surface of the zinc plate after the synthesis at 0.4M electrolyte concentration. There is no trace of ZnO nanostructures. This is attributed to the low formation of OH^- and low ionic conductivity of the electrolyte solution. From the SEM images it is shown that the formation of nano-needle structures starts at 0.5M concentration even though they are superimposed with a nano-flake-like structure. Based on these observations, different samplings were undertaken for consistency as shown in Figure 4.2 (b1) and (b2). From this samplings, it is apparent that the current distribution on the zinc plate was not uniform. This is in agreement with our XRD pattern. However, these

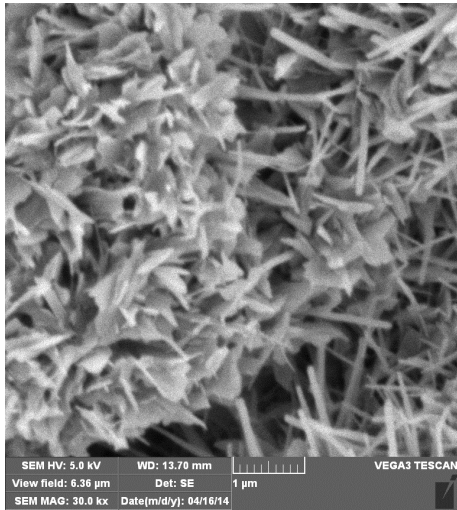
nano-flake structures break into nanoneedles as the concentration increases. This is thought to arise because the higher concentration implies a higher ionic conductivity and concentration of OH^- which then attack the rough surfaces of the nano-flakes. Figure 4.2 (d) shows a low magnification SEM image of the distribution of ZnO nano-structures on the zinc surface. Figure 4.2 (e) shows the formation of clear, sharp-tipped nanoneedles. The length of the obtained nanoneedles as a function of electrolyte concentration was estimated and shown in Figure 4.3. The average nano-needle height is in a range of 780 nm to 2200 nm, which is an indication of good properties of nano needles [77]. Figure 4.3 suggests some dependence of the length of the nanoneedles on electrolyte concentration for concentrations of 0.6M, 1.0M and 2.0M which are above the apparent nano-needle formation threshold 0.5M. The data appears to suggest an increasing nano-needle length with electrolyte concentration. A more detailed study of the length variation with electrolyte concentration is needed. However, Zhang et al [101] report that the morphology and size of ZnO nanorods can be tuned by adjusting the concentration of the electrolyte, the electrodeposition duration and applied current density. They observed that at fixed current density the diameters of the nanorods increased with concentration and that when the electrolyte concentration is increased from 0.5 to 1M the shapes of the self-formed ZnO structures change from cone to hexagon and attributed it to the higher growth speed of the ZnO seeds toward radial direction under higher electrolyte concentration [101]. Similar results of length dependence on electrolyte concentration were obtained by Zhu et al [102].



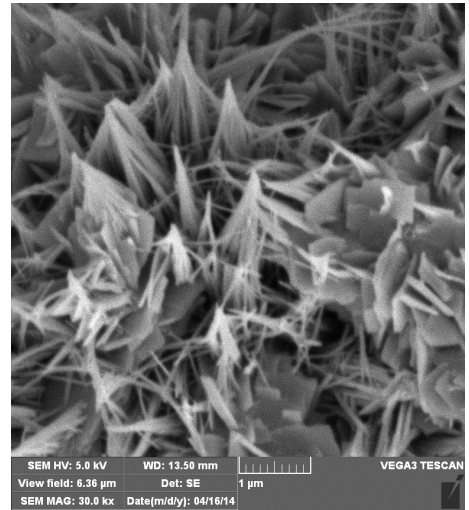
(a)



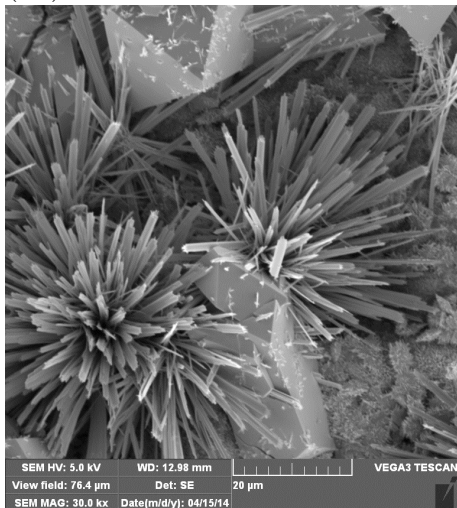
(b1)



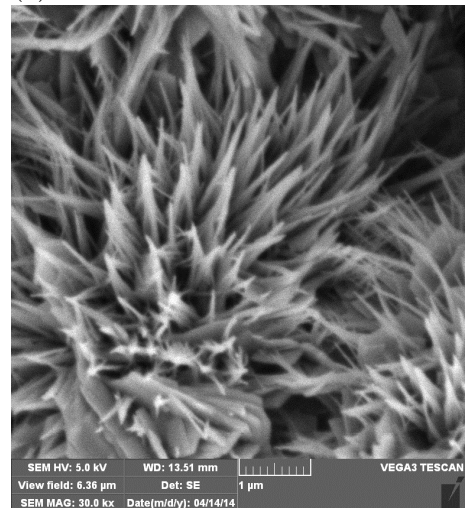
(b2)



(c)



(d)



(e)

Figure 4.2: SEM micrographs at different electrolyte concentrations (a) 0.4M NaOH (b) 0.5M NaOH (c) 0.6M NaOH (d) 1M NaOH (e) 2M NaOH

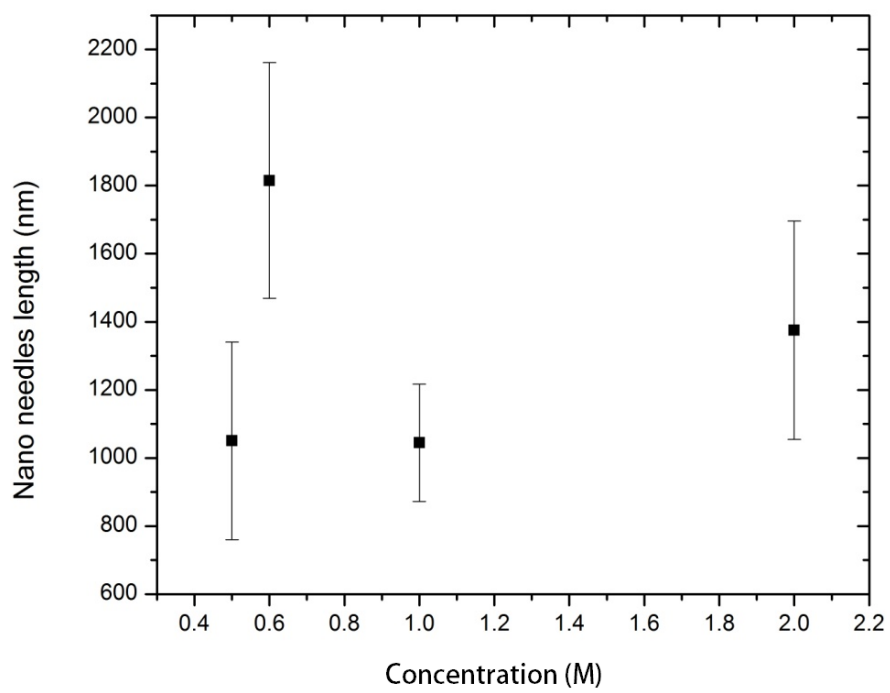


Figure 4.3: Estimation of nano needles length

Chapter 5

Effects of annealing temperature

5.1 Introduction

Over the past decades Zinc Oxide (ZnO) has drawn much research attention due to its unique properties. For instance, it has wide band gap energy of 3.37eV and a large exciton binding energy of 60 meV [37, 103]. It has good transparency, high electron mobility of $\approx 2000 \text{ cm}^2/(\text{Vs})$ at 80 K [104] and it is arguably the richest single semiconductor material in terms of variety of one-dimensional (1-D) nanostructures such as nano-rods, nano-flakes and nanoneedles [52, 105–108]. These properties make this material a potential candidate in many different optoelectronic applications such as solar cells, wave guides, laser diodes and gas sensors [17, 98]. The properties of ZnO nanostructures are interesting because they differ substantially from those of bulk ZnO. Different methods are currently employed to synthesize ZnO nanostructures. Some examples of these methods are the sol-gel, hydrothermal, chemical bath deposition (CBD) electro-deposition, microwave-assisted techniques, chemical vapor deposition (CVD) and precipitation methods [8, 17, 98, 99, 108–111]. XRD studies have shown that this method allows different nanostructures to be obtained depending on the parameter of variation such as discharge

time and type of electrolyte used. In this chapter, we investigate the effect of annealing temperature on the samples synthesized over one hour discharging time using the ZAC system. There is evidence in the literature to suggest that annealing at high temperature potentially plays a number of roles. It is reported that ZnO nanostructures synthesized at room temperatures remain stable even at very high temperatures [99,109]. ZnO nano-structures continue to exhibit a usable, wide band gap of $\approx 3.13\text{eV}$, a decrease of approximately only 7 % of its room temperature band gap at a temperature of 1100°C [109]. This has a promising significance for future semiconductor devices at high temperatures that are comparable to compound semiconductors like silicon carbide with band gap energy of 3.23eV [112]. High temperature annealing of ZnO nano-structures also appears to increase optical properties such as photoluminescence [21], improved crystallinity [113]. Furthermore, annealing at higher temperatures provides a mechanism for the substitution of a zinc atom in the presence of an impurity in a process that is effectively akin to doping ZnO [114]. However, it has also been reported by Hwang et al [115] that annealing resulted in the deterioration of the photoluminescence spectra of ZnO nano-structures when deposited on soda-lime-silica glass substrates rather than zinc. Chin et al [116] have reported an increase in the intensity of the ultraviolet (UV) emission intensity with annealing temperature and dwelling time, in addition to increased crystallization [8, 116–118]. In this chapter the effect of annealing temperature on the structure, morphology and optical properties of the ZAC synthesized ZnO nanoneedles was investigated. The primary aim of the investigation was to evaluate the effect of temperature on the stability of nanoneedles particularly for the use of the nano-needle structures for wide band gap, high temperature devices such as LEDs and a variety of other sensing devices.

5.2 Experimental

5.2.1 Synthesis and annealing

The samples were prepared as described in Chapter 4. The cell was then discharged over one hour into a 470Ω load resistor. After the discharge, the zinc plate was removed and cut into several $1 \times 1 \text{cm}^2$ pieces before annealing. The pieces were placed into an alumina boat that was put in a box-type furnace. The heating was done at different temperatures 400°C , 450°C , 500°C and 600°C for 60mins. Annealing time is known to affect the extent to crystallization [17,98]. The samples were then allowed to cool down naturally back to room temperature prior to characterization.

5.2.2 Characterization

The structure of ZnO nanoneedles was determined using X-ray diffraction (XRD, Bruker AXS D8 Advanced) with $\text{CuK}\alpha$ value of 1.5418\AA radiation. The particle morphology and chemical composition of the samples were then studied using a Joel JSM-9800F Field Emission Scanning electron microscope (FE-SEM) equipped with a dispersive x-ray spectrometer (EDS). The optical properties were studied using a Perkin-Elmer Lambda 950 UV-Vis spectrometer.

5.3 Results and discussion

5.3.1 Structural characterization

Figure 5.1 shows the XRD patterns of ZnO nanoneedles synthesized at different concentrations. The diffraction peaks at scattering angle (2θ) of 31.8° , 34.4° , 36.3° , 47.5° , 56.5° , 62.7° , 66.3° , 67.9° and 69.0° correspond to the reflection

from (100), (002), (101), (102), (110), (103), (200), (112) and (200) crystal planes respectively. These reflections correspond to the standard card (JCPDS: 80-0075) of the hexagonal wurtzite ZnO structure. The other prominent diffraction peaks in the figure are attributed to zinc, confirmed with the JCPDS: 04-0831 standard card of hexagonal structured zinc. No impurities were observed. Figure 5.2, suggests that as the temperature increases the

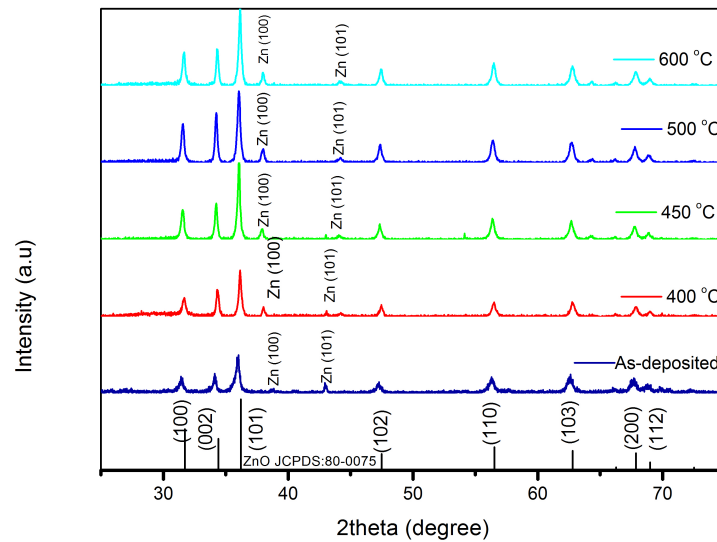


Figure 5.1: XRD pattern of ZnO nanostructures synthesized at different temperatures

diffraction peaks are narrower and exhibit a higher intensity, which further suggests that the nanoneedles become more crystalline. This can be attributed to the change in crystal size. The diffraction peak of (100) was used to plot the graph of intensity versus annealing temperature. It is also found that ZnO nanoneedles synthesized at 450°C gave the optimal intensity. Therefore, majors were taken to estimate particle sizes. Debye-Scherrer equation (3.3.2) was employed to determine the crystalline sizes of ZnO nanoneedles as discussed in previous chapters.

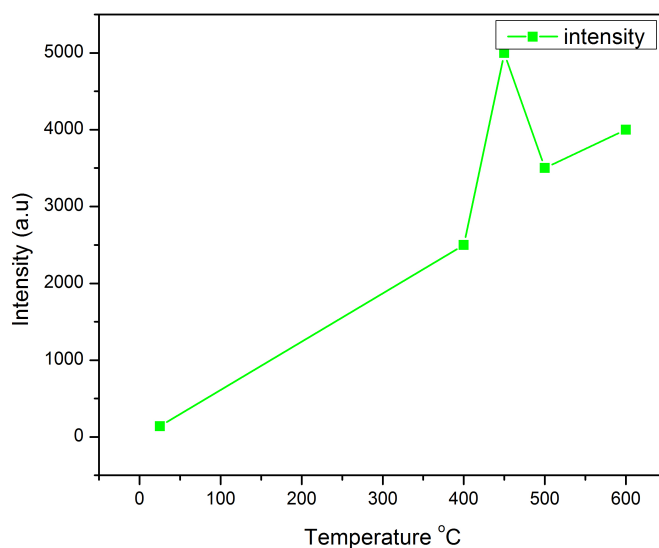


Figure 5.2: Effect of temperature on particle intensity

The crystallite sizes were found to be increasing with the increasing temperature as shown in Figure 5.3, the average particle size was found to be ≈ 25.56 nm. Thus temperature plays an important role in tuning the material crystal sizes. However, the calculated particle size of ZnO nanoneedles synthesized at 450°C gave the optimal particle size which is in agreement with FE-SEM micrographs (Figure 5.4) and optimal intensity (Figure 5.2)

The lattice parameters a (0.327 ± 0.02 nm) and c (0.5662 ± 0.02 nm) for ZnO thin films annealed at different temperature were calculated using Miller indices hkl (equation 4.2.1) and found to be consisted with the standard card JCPDS:80-0075 with lattices $a = 3:2498 \text{ \AA}$ and $c = 5:2066 \text{ \AA}$. The variation of lattice parameters caused by annealing temperature is shown in Table 5.1. From the figure it is observed that as the annealing temperature increases the lattice parameters decreases. The results of Ivetic et al [112] also depict a general reduction in both lattice parameters when the temperature is increased from 700° to 1100° although their work considers the effect of a magnesium

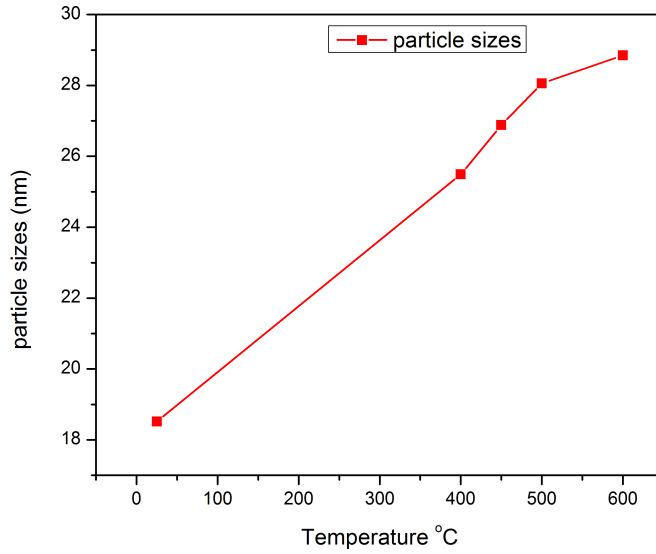


Figure 5.3: Effect of temperature on particle size

impurity atom substituting a zinc atom at a higher temperature. The radius of the magnesium atom is smaller than that of a zinc atom and this explains the reduction of the lattice parameters. In this particular case the lowering of lattice parameters is thought to be the effect of stress undergone by thin film grains and may be due to a change in the nature and concentration of the native imperfections [117]. This causes compression of the lattice parameters. ZnO nanostructures may typically have a number of defects such as oxygen vacancies, lattice disorders, etc. As a result of annealing these defects are removed and the lattice contracts. Also lattice relaxation due to dangling bonds should be taken into account. The dangling bonds on ZnO surface interact with oxygen ions from the atmosphere and due to electrostatic attraction, leading to a lattice that is slightly contracted [117,118].

Table 5.1: Effect of annealing temperature on lattice parameters

Estimated ZnO Parameters			
Annealing temperature (°C)	2θ (degrees)	c (Å)	a (Å)
25	31.4316	5.686	3.283
400	31.6567	5.666	3.271
450	31.5413	5.664	3.270
500	31.5543	5.649	3.261
600	31.6406	5.646	3.360

5.3.2 Surface and chemical composition characterization

Figures 5.4 (a-e) show the FE-SEM micrographs of ZnO nanoneedles annealing from room temperature to 600°C. All the images show randomly orientated nanoneedles with the preferred vertical orientation. As the temperature increases, the nanoneedles appear to be tapered to a sharper end at the top. The average nanoneedle length is in the range 538.1 nm to 1195 nm range, suitable for optoelectronic applications such as solar cells, wave guides, laser diodes and gas sensors and field emitters [119, 120]. Figure 5.5 shows EDS spectrum measurements of the ZnO nanoneedles. It is clear that there are no impurities from other materials besides carbon which can be attributed to either the handling of the sample or as a result of post heating. However, in spite of the EDS spectrum showing three peaks i.e. zinc, oxygen and carbon, the weight percent of Zn, and O elements obtained from EDS is nearly stoichiometric.

5.3.3 Band gap estimation using UV-VIS spectrometer

Figure 5.6 shows the UV-Vis spectra of ZnO nanoneedles synthesized at different annealing temperatures. The ZnO nanoneedles exhibit strong absorption peaks in the range of $\approx 360\text{nm}$ to 380nm , which is attributed to the electronic transition of electrons from valence band to conduction band. This implies

that ZnO nanoneedles are in the regime of spatial excitonic confinement compared to bulk of ZnO. It is observed from the spectra that the absorbance of the samples slightly decrease and the absorption edge slightly shift lower energy. The red shift of the absorption peak could be due to the changes in band gap as an effect of annealing temperatures. The optical absorption of direct band gap ZnO nanoneedles was estimated using Kubelka-Munk function (equation 5.3.1) and Tauc's relation (5.3.2) [120].

$$F(R) = ((1 - R)^2/2R) \quad (5.3.1)$$

$$h\nu = ((F(R)) * h\nu)^2 \quad (5.3.2)$$

Where R is absolute reflectance of the sample layer, $h\nu$ is photon energy (h = Planck's constant and ν = frequency of the photon), $n = 0.5$, since ZnO is a direct band gap semiconductor material. The optical band gap was achieved by extrapolating the steep segment of the sliding curve in a plot of $((F(R)(h\nu))^n$ vs photon energy ($h\nu$) as shown in Figure 5.7.

The estimated band gap E_g was found to be 3.29, 3.28, 3.3 and 3.3 eV for ZnO thin films annealed at 400, 450, 500 and 600°C, respectively. It is observed that the band gap roughly increase with increase in annealing temperature, thought to be due to defects at higher temperatures [121]. There are other factors that explain the increase in energy band gap. For instance the effect of O₂ absorption by the film and referred to as the Burstein-Moss (BM) process [121, 122]. Moustaghfir et al [122] have shown that defects such as O/Zn ratio increases with annealing temperature which leads to variations in the electronic properties. The average estimated optical band gap of ZnO nanoneedles is $\approx 3.3160.05\text{eV}$. Therefore the average estimated optical band gap of ZnO nanoneedles is $\approx 3.316 \pm 0.05\text{eV}$.

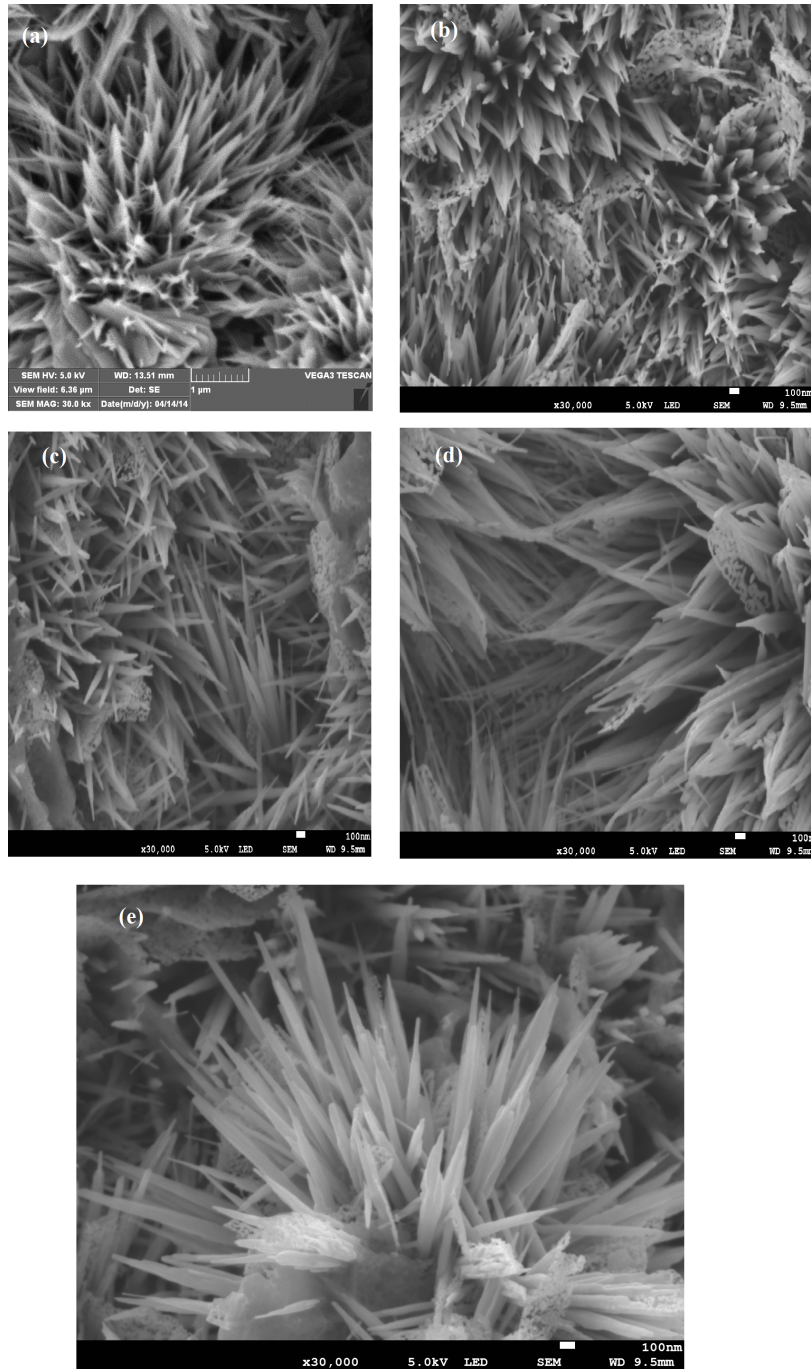


Figure 5.4: SEM images before/after annealing (a) before (b) 400 °C (c) 450 °C (d) 500 °C and (e) 600 °C

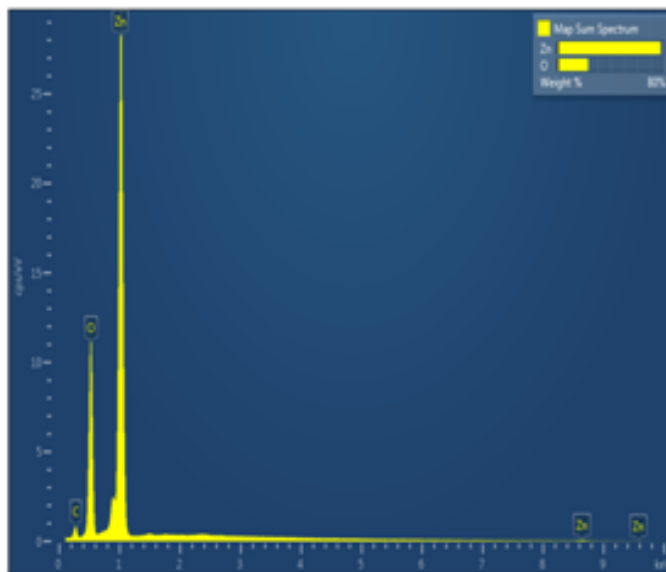


Figure 5.5: Chemical compositions of ZnO nanoneedles

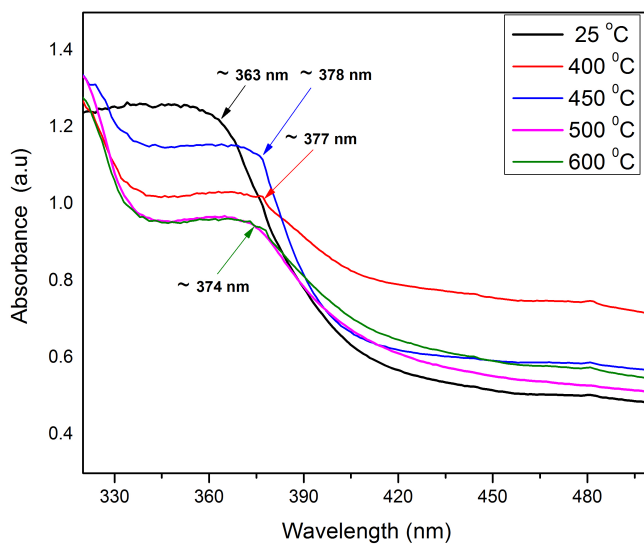


Figure 5.6: UV-Vis absorbance spectra of annealed ZnO nanoneedles.

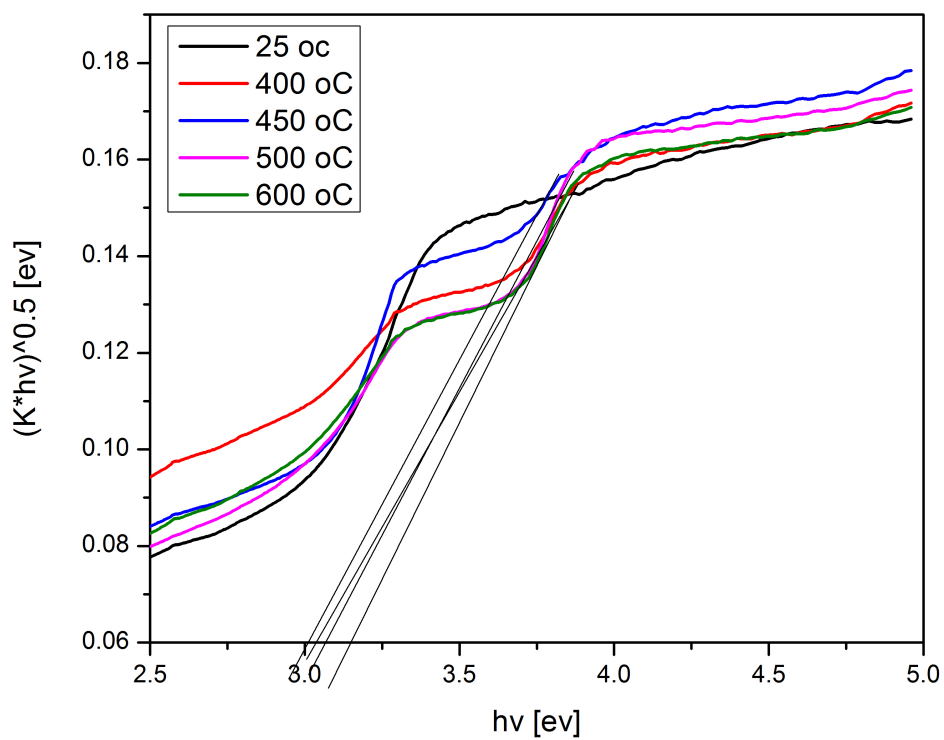


Figure 5.7: Plot of $(F(R) \cdot h\nu)^{0.5}$ vs. photon energy ($h\nu$) of ZnO nanoneedles

Chapter 6

Conclusions

The zinc-air system has been investigated as a possible method of producing ZnO nanoparticles on a zinc plate at room temperature using NaOH as the electrolyte. The ZnO circuit profile shows open-circuit voltages in a range of $\approx 1.2\text{V}$ for all the five different concentrations used. The surface morphological and structural characterization confirms a layer of well-aligned crystalline (ZnO) nano-needles with the particle size varies in a range of 19nm to 39nm. The XRD spectrum shows no diffraction peaks of ZnO synthesized with 0.4M and 0.5M thus following an amorphous nature. There is some correlation between the formation of ZnO structures on the electrode and behavior of the internal resistance and the available energy of the cell with the concentration of the NaOH electrolyte. The variation of the internal resistance of the cell under constant loading conditions is suggested as a possible tool to characterize the useful power output of the cell and its effectiveness for specific applications. Further work is needed to better quantify the effects of the formation of the nano-products and others on the electrodes with respect to the charge transfer performance of the ZAC. This is important for the application of the ZAC cell to powering external devices. It is also interesting to quantify the conditions under which electrical power is maximized with regard to the formation of these products. Furthermore, the effect of annealing temperature

on the structural, morphological and optical properties of synthesized ZnO thin films was investigated using XRD, FE-SEM and UV-vis measurements. XRD measurements indicated that the synthesized ZnO nano-needles exhibit the hexagonal wurtzite structure with no impurities. An increase in height was observed as an effect of annealing temperature. UV-Vis showed an increase in band-gap as increase in heating temperature. Therefore, this method is suitable for some important applications such as LEDs, UV photo detectors, sensing and for other optoelectronic devices.

ZnO nanoparticles offer many advantages in various sectors of science due to their unique properties observed at the nanoscale. Cheaper ways of synthesizing this material will be a great advantage. In this study we have investigated ZAC system as a feasible method of synthesizing ZnO nanoparticles. However, our investigation open wide window for future work. ZnO is one the richest semiconductor material in terms of nanostructures. Therefore, this method should be investigated for the production of these nanostructures. Further majors should be taken into account in future to understand the surface interactions in the ZnO using different electrolytes. Techniques such as FTIR, TEM and XPS should also be included to better understand surface contamination on the zinc plate. The operating conditions should be also adjusted to improve the ZnO crystal structure and maximize ZnO mobility. This could lead to a substantial improvement of the electrical performance of the cell as a standalone unit whose surface products and physics are well understood. In undertaking this research so many research questions were raised which we set out to answer. In attempting to answer these questions, we devised a method to synthesize ZnO nanostructures and used various techniques to characterize them. We were able to answer many of the initial questions, but many new questions arose that promise further work. We learnt

many new tools and techniques during this rewarding research. Finally, the initial part of the work has been presented as a poster to the 59th Annual conference of the South African Institute of Physics (SAIP2014) and was awarded the *best poster prize* in the M.Sc category. Other aspects of the work have been published in a high-impact scientific journal. Details of which are given below.

6.0.4 Publications

1. T.D Malevu and R.O Ocaya 2014. *Synthesis of ZnO Nanoparticles Using a Zinc-Air Cell and Investigation of the Effect of Electrolyte Concentration*, Int. J. Electrochem. Sci., Vol. 9 (12) pp. 8011-8023.
2. T.D Malevu and R.O Ocaya 2015. *Effect of Annealing Temperature on Structural, Morphology and Optical Properties of ZnO Nano-Needles Prepared by Zinc-Air Cell System Method*, Int. J. Electrochem. Sci., Vol. 10 (2) pp. 1752-1761.
3. T.D Malevu and R.O Ocaya 2014. *Poster presented at The 59th Annual Conference of the SA Institute of Physics (SAIP2014)*, University of Johannesburg. *Best M.Sc poster award.*

References

- [1] Nowack., B., Bucheli, T.D., 2007. Occurrence, behavior and effects of nanoparticles in the environment, *Journal of Environmental Pollution* 150 (1): 5-22
- [2] Freestone, I., Meeks, N., Sax, M., Higgitt, C., 2007. The Lycurgus Cup - A Roman nanotechnology, *Gold Bulletin* 40(4):270-277.
- [3] Helland, A. 2004. Nanoparticles: A Closer Look at the Risks to Human Health and the Environment, *The International Institute for Industrial Environmental Economics*, Sweden. Online thesis.
- [4] Zainelabdin, A.E.E., 2012. Lighting and Sensing Applications of Nanostructured ZnO, CuO and Their Composites Ahmed Eltahir Elsharif Zainelabdin, Linkping University, SE-601 74 Norrkping Sweden. Online thesis.
- [5] Groso, A., Petri-Fink, A., Magrez, A., Riediker, M., Meyer, T., 2010. Management of nanomaterials safety in research environment, *Journal of Particle and Fibre Toxicology* 7(1):40.
- [6] Choi, K., 2003. Ethical issues of nanotechnology development in the Asia pacific region, Ewha Womans University for the Regional Meeting on Ethics of Science and Technology.
- [7] Roland, D. Harrison, R.D., Leigh-Jarvis, A.L., Sergio Babet, S., 2013. A Simple Microwave Plasma-Enhanced Chemical Vapour Deposition System for the Production of Carbon Nanotubes *In Proceedings of the*

IEEE Africon 2013, IEEE Catalog Number CFP13AFR-PRT, pp. 967-970.

- [8] Yap, C.K., Tan, W.C., Alias, S.S. and Mohamad, A.A. 2009. Synthesis of zinc oxide by zinc-air system, *Journal of Alloys and Compounds* 484: 934-938.
- [9] Chen, D., Wang, K., Xiang, D., Zong, R., Qa, W., Zhu, Y., 2014. Significantly enhancement of photocatalytic performances viacore-shell structure of ZnO@mpg-C3N4, *Journal of applied Catalysis B: Environmental* 147: 554- 561.
- [10] Raja, K., Ramesh, P.S., Geetha, D., 2014. Synthesis, structural and optical properties of ZnO and Ni-doped ZnO hexagonal nanorods by Co-precipitation method, *Spectrochimica Acta Part A: Molecular and Biomolecular Spectroscopy* 120: 19-24.
- [11] Rupasinghe, R.P., 2011. Dissolution and aggregation of zinc oxide nanoparticles at circumneutral pH; a study of size effects in the presence and absence of citric acid, University of Iowa. online Thesis and Dissertations
- [12] Lue, J.T., 2007. Physical properties of nanomaterials), *H.S. Nalwa (Ed.),Encyclopedia of Nanoscience and Nanotechnology* 10:1-46.
- [13] Deng, W.Q., 2004. Computational aided design in molecular nanotechnology, *California Institute of Technology Pasadena*, California. online thesis
- [14] Bennett, T.J., 2013. Nanomaterials - A miniscule introduction, *Katherine A. Kelley State Public Health Laboratory APHL Annual Meeting*. APHL Annual Meeting
- [15] Fauss, E.K., 2008. Risk analysis of nanotechnology through expert elicitation: A silver nanotechnology study, University of Virginia. online thesis

- [16] Mohanraj, V.J., Chen, Y., 2006. Nanoparticles - A Review, *Tropical Journal of Pharmaceutical Research* 5(1): 561-573.
- [17] Chen, Z., Li, X.X., Du, G., Chen, N., Suen, A.Y.M., 2011. A sol-gel method for preparing ZnO quantum dots with strong blue emission, *Journal of Luminescence* 131(10):2072-2077.
- [18] Bhutt, I., Tripathi, B.N., 2011. Interaction of engineered nanoparticles with various components of the environment and possible strategies for their risk assessment, *Chemosphere* 82(3): 308-317.
- [19] Sau, T., Rogach, A.L., Jackel, F., Klar, T.A., Feldmann, J., 2010. Properties and Applications of Colloidal Nonspherical Noble Metal Nanoparticles, *Advance Materials* 22(16):1805-1825.
- [20] Paulus, P.M., Goossens, A., Thiel, R.C., van der Kraan, A. M. Schmid, G., de Jongh, L. J. 2001. Surface and quantum-size effects in Pt and Au nanoparticles probed by ^{197}Au Mossbauer spectroscopy, *Physical Review B* 64:205418.
- [21] Yang, H.M., Park, C.W., Ahm, T., Jung, B., Seo, B., Park, H., Kim, J.D., 2013. A direct surface modification of iron oxide nanoparticles with various poly(amino acid)s for use as magnetic resonance probes, *Journal of Colloid and Interface Science*, 1;391: 158-167.
- [22] Mazhdi, M., Saydia, J., Karimib, M., Seidid, J., Mazhdi, F., 2013. A study on optical, photoluminescence and thermoluminescence properties of ZnO and Mn doped-ZnO nanocrystalline particles, *Optik - International Journal for Light and Electron Optics* 124(20): 4128-4133.
- [23] Subhasree, R. S., Selvakumar D., Kumar, N. S., 2012. Hydrothermal mediated synthesis of ZnO nanorods and their antibacterial properties, *Open Access Journal Letters in Applied NanoBioscience* 1(1):002-007.

- [24] Garcia, M.F., Rodriguez, J. A., 2007. Metal Oxide nanoparticles, *Nanomaterials: Inorganic and Bioinorganic Perspectives*: BNL-79479-2007-BC.
- [25] Tan, W.C. and Mohamad, A.A. 2010. A Study on the Effects of the Discharge Current and Ambient Temperature on the Formation of Zinc Oxide Synthesized via the Zinc-Air System, *Journal of The Electrochemical Society* 157(12): E184-E190.
- [26] Szalay, B., 2012. Iron oxide nanoparticles and their toxicological effects: In Vivo and in vitro studies, University of Szeged, Szeged. online thesis
- [27] Pejova, B., 2014. Optical phonons in nanostructured thin films composed by zincblende zinc selenide quantum dots in strong size-quantization regime: Competition between phonon confinement and strain-related effects, *Journal of Solid State Chemistry* 213: 2231.
- [28] Jacobsson, T.J., 2010. Synthesis and characterization of ZnO nanoparticles. An experimental investigation of some of their size dependent quantum effects, Uppsala University Sweden. online thesis
- [29] Liu, X., Zhong, Z., Tang, Y., Liang, B., 2013. Review on the Synthesis and Applications of Fe₃O₄ Nanomaterials, *Journal of Nanomaterials*, Article ID 902538: 7pages.
- [30] Thereja, R.K., Shukla, S., 2007. Synthesis and characterization of zinc oxide nanoparticles by laser ablation of zinc in liquid, *Applied Surface Science* 253(22): 8889-8895.
- [31] Ibupoto, Z.H., Khun, K., Erksson, M., AlSalhi, M., Atif, M., Ansari, A., Willander, M., 2013. Hydrothermal Growth of Vertically Aligned ZnO Nanorods Using a Biocomposite Seed Layer of ZnO Nanoparticles, *Materials* 6(8): 3584-3597.

- [32] Ghaffarian, H.A., Saiedi, M., Sayyadnejad, M.A., Rasgid, A.M., 2011. Synthesis of ZnO Nanoparticles by Spray Pyrolysis Method, *Iranian Journal of Chemistry and Chemical Engineering* 30(1): 1-6.
- [33] Khanpour, M., Marsali, A., 2010. Synthesis and characterization of ZnS and ZnO nanoparticles via Thermal decomposition of two new synthesized one dimensional coordination polymers at two different temperatures, *Journal of Inorganic and Organometallic Polymers and Materials* 20:692-697.
- [34] Jayalakshmi, M., Palaniappa, M., Balasubramanian, K., 2008. Single Step Solution Combustion Synthesis of ZnO/carbon Composite and its Electrochemical Characterization for Supercapacitor Application, *Journal of International Electrochemical Science* 3:96-103.
- [35] Maity, D., Agrawal, D.C., 2007. Synthesis of iron oxide nanoparticles under oxidizing environment and their stabilization in aqueous and non-aqueous media, *Journal of Magnetism and Magnetic Materials* 308(1): 46-55.
- [36] Govendor, Y., 2012. "Isolation, purification and characterization of a 'factor' from fusarium oxysporum responsible for platinum nanoparticles formation.:", Rhodes university, Western Cape. online thesis
- [37] Li, P., Miser, D.E., Rabiei, S., Tadav, R.T., Hajaligol., M.R., 2003. The removal of carbon monoxide by iron oxide nanoparticles, *Applied Catalysis B: Environmental* 43(2): 151-162.
- [38] Singh, M., Ulbrich, P., Prokopec, v., Svoboda, P., Stepanek, F., 2013. Vapour phase approach for iron oxide nanoparticle synthesis from solid precursors, *Journal of Solid State Chemistry*, 200:150-156.
- [39] Misra, S.K., Nuseibeh, S., Dybowska, A., Berhanu, D., Tetley, T.D., Valsami-Jones, E., 2014. Comparative study using spheres, rods and

spindle-shaped nanoplatelets on dispersion stability, dissolution and toxicity of CuO nanomaterials, *Nanotoxicology* 8(4): 422-432

- [40] Ghosh, S.P., 2012. Synthesis and characterization of zinc oxide nanoparticles by sol gel process, National Institute of Technology, Rourkela.
- [41] Kumar, S.S., Venkateswarlu, P., Rao, V.R., Rao, G.N., 2013. Synthesis, characterization and optical properties of zinc oxide nanoparticles, *International Nano Letters* 3:30.
- [42] Scopus, "ZnO related papers", <http://www.scopus.com/> last accessed: March. 2014.
- [43] Behera, J.K., 2009. Synthesis and Characterization of ZnO nanoparticles, Department of physics national institute of technology, Rourkela. online thesis
- [44] Wang, Z.L, 2004. Zinc oxide nanostructures: growth, properties and applications, *Journal of Physics: Condensed Matter* 16: R829-R858
- [45] Chen, X.C., Zhou, J.P., Wang, H.Y., Xu, P.S., pan, G.Q., 2011. In situ high temperature X-ray diffraction, *Journal of Chinese Physics B*, 20(9):096102
- [46] Long, W., Yang,Z., Fan, X., Yang, B., Zhao, Z, Jing, J., 2013. The effects of carbon coating on the electrochemical performances of ZnO in NiZn secondary batteries, *Electrochimica Acta* 105: 40 46.
- [47] Shakti, N., Gupta, P.S., 2010. Structural and Optical Properties of Sol-gel Prepared ZnO Thin Film, *Applied Physics Research* 2(1): 1928.
- [48] Talam, S., Karumuri, S.R., Gunnam, N., 2012. Synthesis, Characterization, and Spectroscopic Properties of ZnO Nanoparticles, *International Scholarly Research Network ISRN Nanotechnology*, volume 2012 Article ID 372505: 6 pages

- [49] Fan, Z.Y., Lu, J.G., 2005. Zinc oxide nanostructures: Synthesis and properties, *Journal of Nanoscience and nanotechnology* 5(10):1561-157.
- [50] Yufei, Z., Zhiyou, G., Xiaoqi, G., Dongxing, G., Yunxiao, D., Hongtao, Z., 2010. First-principles of wurtzite ZnO (0001) and (0001) surface structures, *Journal of Semiconductors*31(8):DOI: 10.1088/1674-4926/31/8/082001.
- [51] Barreca, D., Bekermann, D., Cominic, E., Devi, A., Fischer, R.A., Gasparotto, A., Maccato, C., Sberveglieric, G., Tondellod, E., 2010. 1D ZnO nano-assemblies by Plasma-CVD as chemical sensors for flammable and toxic gases, *Sensors and Actuators B* 149(1-6): 17.
- [52] Kim, H., Kim, H., Kim, D., 2014. Effect of oxygen plasma treatment on the electrical properties in Ag/bulk ZnO Schottky diodes, *Vacuum*101: 92-97.
- [53] Kim, K., Son, H., Choi, N., Kim, J., Lee, S., 2013. Growth and characterization of polar and nonpolar ZnO film grown on sapphire substrates by using atomic layer deposition, *Thin Solid Films* 546: 114-117.
- [54] Thomas, D.G., 1960. The exciton spectrum of zinc oxide, *Journal of Physics and Chemistry of Solids* 15(1-2):86-96.
- [55] Hopfeld, J.J., 1960. Fine structure in the optical absorption edge of anisotropic crystal, *Journal of physics and chemistry of solids* 15(1-2):97-107.
- [56] Hutson, A.R., 1961. Piezoelectric scattering and phonon drag in ZnO and Cds, *Journal of Applied Physics* 32(10):2287-2292.
- [57] Behera, O., 2011. Synthesis and Characterization of ZnO nanoparticles of various sizes and Applications in Biological systems, National Institute of Technology, Rourkela. online thesis

- [58] Avrutin, V., Cantwell, G., Zhang, J.Z., Song, J.J., Silversmith, D.J., Morkoc, H., 2010. A brief overview of the recent achievements in mass production of ZnO single crystals, *Proceedings of the IEEE* 98: 13391350
- [59] Park, W.I., Jun, Y.H., Jung, S.W., Yi, G., 2002. Excitonic emission observed in ZnO single crystal nanorods, *Journal of Applied Physics letters* 82(6):964.
- [60] Hassan, M.M., Khan, W., Azam, A., Naqvi, A.H., 2014. Effect of size reduction on structural and optical properties of ZnO matrix due to successive doping of Fe ions, *Journal of Luminescence* 145: 160166.
- [61] Pinto, Y., van der Leij, A.R., Sligte, I.g., Lamme, V.A.F., Steven Scholte, H., 2013. Bottom-up and top-down attention are independent, *Journal of Vision* 13(3):16, 114
- [62] Buitrago, E., Fernandez-Bolaos, M., Rigante, S., Zilch, C.F., Schrter, N.S., Nightingale, A.M., Ionescu, A.M., 2014. The top-down fabrication of a 3D-integrated, fully CMOS-compatible FET biosensor based on vertically stacked SiNWs and FinFETs, *Sensors and Actuators, B: Chemical* 193:400-412
- [63] Bidet-Caulet, A., Bottemanne, L., Fonteneau, C., Giard, M.-H., Bertrand, O., 2014. Brain Dynamics of Distractibility: Interaction Between Top-Down and Bottom-Up Mechanisms of Auditory Attention, *Brain Topogr* DOI 10.1007/s10548-014-0354-x:Pages 1-14
- [64] Cheng, X.L., Rong, Z., Zhang, X.F., Xu, Y.M., Gao, S., Zhao, H., Huo, L.H., 2013. In situ assembled ZnO flower sensors based on porous nanofibers for rapid ethanol sensing, *Sensors and Actuators, B: Chemical* 188: 425-432
- [65] Yang, Y., Li, Y., Zhu, L., He, H., Hu, L., Huang, J., Hu, F., He, B., Ye, Z., 2013. Shape control of colloidal Mn doped ZnO nanocrystals and their visible light photocatalytic properties, *Nanoscale* 5(21): 10461-10471

- [66] Mino, L., Agostini, G., Borfecchia, E., Gianolio, D., Piovano, A., Gallo, E., Lamberti, C., 2013. Low-dimensional systems investigated by x-ray absorption spectroscopy: A selection of 2D, 1D and 0D cases, *Journal of Physics D: Applied Physics* 46(42): Article number 423001. doi:10.1088/0022-3727/46/42/42300
- [67] Birol, H., Rambo, C.R, Guiotoku, M and Dachamir Hotza, D., 2013. Preparation of ceramic nanoparticles via celluloseassisted glycine nitrate process: a review, *Journal of Royal Society of Chemistry* 3:2873-2884
- [68] Wang, L., Xu, L., Kuang, H., Xu, C., Kotov, N.A., 2011. Dynamic Nanoparticle Assemblies, *Accounts of Chemical Research* 45(11): 19161926
- [69] Triboulet, R., 2014. Growth of ZnO bulk crystals: A review, *Progress in Crystal Growth and Characterization of Materials* 60(1):1-14
- [70] Yu ,D., Trad, T., McLeskey, J.T., Cracium, V., Taylor, C., 2010. ZnO Nanowires Synthesized by Vapor Phase Transport Deposition on Transparent Oxide Substrates, *Journal of Nanoscale Research Letters* 5(8): 13331339.
- [71] Kim, Y.H., Heo, J.S., Kim, T.H., Park, S., Yoon, M.H., Kim, J., Oh, M.S., Yi, G.R., Nod, Y.Y., Park, S.K., 2012. Flexible metal-oxide devices made by room-temperature photochemical activation of solgel films, *Nature Internanational Journal of Science* 489: 128132
- [72] Yu, S., Zhang, W., Li, L., Dong, H., Xu, D., Jin, Y., 2014. Structural, electrical, photoluminescence and optical properties of ntype conducting, phosphorus-doped ZnO thin films prepared by pulsed laser deposition, *Applied Surface Science* 298:4449
- [73] Wu, M., Yu, S., He, L., Zhang, G., Ling, D., Zhang, W., 2014. Influence of oxygen pressure on the structural, electrical and optical properties of

Nb-doped ZnO thin films prepared by pulsed laser deposition, *Applied Surface Science* 292: 219-224.

- [74] Kathalingam, A., Ambika, N., Kim, M.R., Elanchezhiyan, J., Chae, Y.S., Rhee, J.K., 2010. Chemical bath deposition and characterization of nanocrystalline ZnO thin films, *Materials Science-Poland* 28(2) 513.
- [75] Fujimoto, K., Oku, T., Akiyama, T., 2013. Fabrication and Characterization of ZnO/Cu₂O Solar Cells Prepared by Electrodeposition, *Applied Physics Express* 6(8):086503
- [76] Lan, C.J., Chin, T.S., Lin, P.H., Perng, T.P., 2004. Zn-Al alloy as a new anode-metal of a zinc-air battery, *Journal of New Materials for Electrochemical Systems* 9: 27-32
- [77] Mohamad, A.A., 2006. Zn/gelled 6M KOH/O₂ zinc.air battery, *Journal of Power Sources* 159: 752.757
- [78] Huang, X., 2014. Performance evaluation of a non-woven lithium ion battery separator prepared through a paper-making process, *Journal of Power Sources* 256: 96101
- [79] Wong, C.S., Bennett, N.S., Manassis, D., Danilewskyc, A., McNally, P.J., 2014. Non-destructive laboratory-based X-ray diffraction mapping of warpage in Si die embedded in IC packages, *Microelectronic Engineering* 117:4856.
- [80] Ben Raben, M., Chaglabou, N., kanzari, M., Bezig, B., 2009. Structural and optical studies on antimony and zinc doped CuInS₂ thin films, *Journal of Physics Procedia* 2(3):745750. <http://dx.doi.org/10.1016/j.phpro.2009.11.020>.
- [81] Myscope., 2014. Training for advance research, *Australian microscopy and microanalysis research facility*. Online. <http://www.ammrf.org.au/> : last accessed: March 2014.

- [82] Chiang, C.-T., DeLeon, R.L., Garvey, J.F., Preparation of Zinc Oxide Thin Films by Reactive Pulsed Arc Molecular Beam Deposition, *Journal of Physical Chemistry* 111 (48): 1770017704 (DOI: 10.1021/jp070898f)
- [83] Chung, B.-H., Kim, S.J., Choi, M. S., Jang, D.Y., 2013. Design and fabrication of a scanning electron microscope (SEM) with an electrostatic column for process embedment, *Journal of the Korean Physical Society* 63(7): 1287-1290
- [84] Song, Yongxiu., Zhu, Jiaxiang., Xu, Hui., 2014. Synthesis, characterization and visible-light photocatalytic performance of Ag₂CO₃ modified by graphene-oxide, *Journal of Alloys and Compounds* 592: 258265
- [85] Sperandio, C., Arnoult, C., 2010. Characterization of the interphase in an aluminium/epoxy joint by using controlled pressure scanning electron microscopy coupled with an energy dispersive X-ray spectrometer, *Micron* 41(2): 105111
- [86] Indiana University Bloomington, 2014. Environmental scanning electron microscope, <http://nano.indiana.edu/QuantaFEGmicro.html>, online 2014.
- [87] <http://cnx.org/contents/ba27839d-5042-4a40-afcf-c0e6e39fb454@19.1:100>, online. September 2014
- [88] Xia, C., Wang, F., Hu, C., 2014. Theoretical and experimental studies on electronic structure and optical properties of Cu-doped ZnO, *Journal of Alloys and Compounds*, 589:604-608
- [89] Safa, S., Mamoori, R., Azimirad, R., 2014. Investigation of reduced graphene oxide effects on ultra-violet detection of ZnO thin film, *Physica E: Low-dimensional Systems and Nanostructures*, 57: 155-160

- [90] Anas, S., Metz, R., Sanoj, M.A., Mangalaraja, R.V., Ananthakumar, S., 2010. Sintering of surfactant modified ZnO-Bi₂O₃ based varistor nanopowders, *Ceramics International*, 36(8): 2351-2358
- [91] Panchayri, V., Kern, K., Balasubramanian, K., 2010. Template-free self-assembly of hierarchical ZnO structures from nanoscale building blocks, *Journal of Chemical Physical letters* 498(4-6): 317-322
- [92] Zacharopoulou, O., Varvaresou, A., 2012. Nanotechnology in cosmetology, *Epitheorese Klinikes Farmakologias kai Farmakokinetikes*, 30(1): 51-54
- [93] Bhattacharya, A., Rao, V.P., Jain, C., Ghose, A., Banerjee., 2014. Bio-sensing properties of gold coated ZnO nanorods, *Materials Letters*, 117:128-130
- [94] Huang, H., Zhao, Q., Hong, K., Xu, Q., Huang, X., 2014. Optical and electrical properties of N-doped ZnO heterojunction photodiode, *Physica E: Low-dimensional Systems and Nanostructures*, 57: 113-117
- [95] Li, J., Guo, D., Wang, X., Wang, H., Jiang, H., Chen, B., 2010. The photodynamic effect of different size ZnO nanoparticles on cancer cell proliferation in vitro, *Nanoscale research letters*, 5(6): 1063-1071
- [96] Saleem, M., Fang, L., Wakeel, A., Rashad, M., Kpng, C.Y., 2012. Simple preparation and characterization of Nano-crystalline Zinc Oxide Thin films by Sol-Gel Method on Glass Substrate, *Journal of Condense Matter Physics*, 2: 10-15
- [97] Ahmed, F., Kumar, S., Arshi, N., Anwar, M.S., Prakash, R., 2011. Growth and characterization of ZnO nanorods by microwave-assisted route: green chemistry approach, *Advanced Materials Letters*, 2(3): 183-187
- [98] Yilmaz, S., 2013. Study of influence of annealing time on some physical properties of ZnO:Cu nanorods grown by a simple chemical bath

deposition, *Journal of Superconductivity and Novel Magnetism*, : 27 (4): 1083-1089

- [99] Chong, S.K., Dee, C.F., Rahman, S.A., 2013. Structural and photoluminescence studies on catalytic growth of silicon/zinc oxide heterostructures nanowires, *Nanoscale Research Letters*, 8:174
- [100] Mathew, J.P., Varghese, G., Mathew, J., 2012. Effect of post-thermal annealing on the structural and optical properties of ZnO thin films prepares from a polymer precursor, *Chinese Physics B*, 21(7) : 078104
- [101] Tak, Y., Yong, K., Park, C., 2005. Selective growth of ZnO nanoneedles on Si substrates by metalorganic chemical vapor deposition, *Journal of Crystal Growth*, 285(4): 549-554
- [102] Y.Q. Zhu, G.T. Fei, Y. Zhang, X.M. Chen, H.B. Tang and L.D. Zhang, 2011. Two-Step Synthesis of ZnO Rod-Needle Nanostructures Using a ZnS Source *Journal of Physical Chemistry C* 115(28):13597-13602
- [103] Pyne, E., Sahoo, G.P., Bhui, K., Bar, H., Sarkar, P., Samanta, S., Maity, A., Misra, A., 2012. Enhanced photocatalytic activity of metal coated ZnO nanowires, *Spectrochimica Acta Part A: Molecular and Biomolecular Spectroscopy*, 93: 100-105
- [104] Srikant, V. and Clarke, D. R., 1998. On the optical band gap of zinc oxide, *Journal of Applied Physics*, 83: 5447-5451
- [105] Baviskar, P.K., Nikam, P.R., Gargote, S.S., Ennaoui, A., Sankapal, B.R., Controlled synthesis of ZnO nanostructures with assorted morphologies via simple solution chemistry, *Journal of Alloys and Compounds*, 551: 233-242
- [106] Cho, S., 2009. Effects of Growth Temperature on the Properties of ZnO Thin Films Grown by Radio-frequency Magnetron Sputtering, *Journal of Transactions on Electrical and Electronic Materials*, 10(6):1-4

- [107] Sheini, F.J., Singh, J., Srivasatva, O.N., Joag, D.S., More, M.A., Electrochemical synthesis of Cu/ZnO nanocomposite films and their efficient field emission behaviour *Applied Surface Science*, 256: 2110-2114
- [108] Dong, J.J., Zhen, C.H., Hao, H.Y., Xing, J., Zhang, Z.L., Zheng, Z.Y., 2013. Controllable synthesis of ZnO nanostructures on the Si substrate by a hydrothermal route *Nanoscience Research Letters*, 8:378
- [109] Xiang-Cun, C., Jie-Ping, Z., Hai-Yang, W., Peng-Shou, X and Guo-Qiang, P., 2011. In situ high temperature X-ray diffraction studies of ZnO thin film, *Chinese Physica B*, 20: 096102: 1-3
- [110] Malevu., T.D., Ocaya, R.O., Synthesis of ZnO Nanoparticles Using a Zinc-Air Cell and Investigation of the Effect of Electrolyte Concentration, *International Journal of Electrochemical Science*, 9: 8011-8023
- [111] Miao, T.T., Sun, D.X., Guo, Y.R, Li, C., Ma, Y, L., Fang, G.Z., Pan, Q.J., 2013. Low temperature precipitation synthesis of flower like ZnO with lignin amine and its optical properties, *Journal of Nanoscale Research Letters*, 8:431
- [112] Ivetic, T.B. , Dimitrievska, M.R., Fincur, N.L., Dacanin, Lj.R., Gth, I.O., Abramovic, B.F and Lukic-Petrovic, S.R., 2014. Effect of annealing temperature on structural and optical properties of Mg-doped ZnO nanoparticles and their photocatalytic efficiency in alprazolam degradation, *Ceramics International* 40(1): 15451552
- [113] Ghafouri, V., Ebrahimzad, A. and Shariati, M., 2013, The effect of annealing time and temperature on morphology and optical properties of ZnO nanostructures grown by a self-assembly method, *Scientia Iranica F* 20(3): 1039-1048 doi: 10.1016/j.scient.2013.02.025
- [114] Wang, C., Ma, S., Sun, A., Qin, R., Yang, F., Li, X., Li, F., Yang,

- X., 2014. Characterization of electrospun Pr-doped ZnO nanostructure for acetic acid sensor, *Sensors and Actuators B: chemical* 193: 326333
- [115] Hwang, K.S., Lee, Y.J. and Hwangbo, S., 2007. Growth, structure and optical properties of amorphous or nano-crystalline ZnO thin films prepared by pre-firing-final annealing, *Journal of Ceramic Processing Research*, 8(5): 305-311.
- [116] Chin, H.S. and Chao, L.S., 2013. The Effect of Thermal Annealing Processes on Structural and Photoluminescence of Zinc Oxide Thin Film, *Journal of Nanomaterials*, Volume 2013 (2013), Article ID 424953, 8 pages, doi: 10.1155/2013/424953
- [117] Usseinov, A.B., Kotomin, E.A., Akilbekov, A.T., Zhukovskii, Y.F., Puans, J., 2014. Hydrogen induced metallization of ZnO (11 00) surface: Ab initio study, *Thin Solid Films*, 553: 38-42
- [118] Chang, J., Muhammad, Z.A., Wlodarski, W., Waclawik, E.R., 2013. Self-Assembled 3D ZnO Porous Structures with Exposed Reactive 0001 Facets and Their Enhanced Gas Sensitivity, *Sensor*, 13 : 8445-8460
- [119] Han, Z., Lia, L., Wu, Y., Pan, H., Shen, S., Chen, J., 2012. Synthesis and photocatalytic application of oriented hierarchical ZnO flower-rod architectures, *Journal of Hazardous Materials*, 217- 218: 100- 106
- [120] Kara, K., Tuzemen, E.S.E., Esen, R., 2014. Annealing effects of ZnO thin films on p-Si(100) substrate deposited, *Turkish Journal of Physics* 38: 238 - 244
- [121] Bouhssira, N., Abed, S., Tomasella, E., Cellier, J., Mosbah, A., Aida, M.S., Jacquet, 2006. Influence of annealing temperature on the properties of ZnO thin films deposited by thermal evaporation, *Applied Surface Science*, 252(15) 5594-5597
- [122] Moustaghfir, A., Tomasella, E., Ben Amor, S., Jacquet, M, Cellier, J., Sauvage, T., 2003. Structural and optical studies of ZnO thin films

deposited by r.f. magnetron sputtering: influence of annealing, *Surface and Coatings Technology*, 174-175(2003) 193-196